An experimental and chemical kinetic modeling study of 1,3-butadiene combustion: Ignition delay time and laminar flame speed measurements

Chong-Wen Zhou [a,b,*], Yang Li [a], Ultan Burke [a], Colin Banyon [a], Kieran P. Somers [a],
Shuiting Ding [b], Saadat Khan [c], Joshua W. Hargis [c], Travis Sikes [c], Olivier Mathieu [c],
Eric L. Petersen [c], Mohammed AlAbbad [d], Aamir Farooq [d], Youshun Pan [e], Yingjia Zhang [e],
Zuohua Huang [e], Joseph Lopez [f], Zachary Loparo [f], Subith S. Vasu [f], Henry J. Curran [a]

[a] Combustion Chemistry Centre, School of Chemistry and Ryan Institute, National University of Ireland Galway, Ireland
[b] School of Energy and Power Engineering, Beihang University, Beijing 100191, PR China
[c] Department of Mechanical Engineering, Texas A&M University, College Station, TX, United States
[d] Clean Combustion Research Center, Division of Physical Sciences and Engineering, King Abdullah University of Science and Technology (KAUST), Thuwal, Saudi Arabia
[e] State Key Laboratory of Multiphase Flow in Power Engineering, Xi'an Jiaotong University, Xi'an 710049, PR China
[f] Center for Advanced Turbomachinery and Energy Research (CATER), Mechanical and Aerospace Engineering, University of Central Florida, Orlando, FL, United States

ARTICLE INFO

ABSTRACT

Ignition delay times for 1,3-butadiene oxidation were measured in five different shock tubes and in a rapid compression machine (RCM) at thermodynamic conditions relevant to practical combustors. The ignition delay times were measured at equivalence ratios of 0.5, 1.0, and 2.0 in 'air' at pressures of 10, 20 and 40 atm in both the shock tubes and in the RCM. Additional measurements were made at equivalence ratios of 0.3, 0.5, 1.0 and 2.0 in argon, at pressures of 1, 2 and 4 atm in a number of different shock tubes. Laminar flame speeds were measured at unburnt temperatures of 295 K, 359 K and 399 K at atmospheric pressure in the equivalence ratio range of 0.6–1.7, and at a pressure of 5 atm at equivalence ratios in the range 0.6–1.4. These experimental data were then used as validation targets for a newly developed detailed chemical kinetic mechanism for 1,3-butadiene oxidation.

A detailed chemical kinetic mechanism (AramcoMech 3.0) has been developed to describe the combustion of 1,3-butadiene and is validated by a comparison of simulation results to the new experimental measurements. Important reaction classes highlighted via sensitivity analyses at different temperatures include: (a) $\dot{O}H$ radical addition to the double bonds on 1,3-butadiene and their subsequent reactions. The branching ratio for addition to the terminal and central double bonds is important in determining the reactivity at low-temperatures. The alcohol-alkene radical adducts that are subsequently formed can either react with $H\dot{O}_2$ radicals in the case of the resonantly stabilized radicals or O_2 for other radicals. (b) $H\dot{O}_2$ radical addition to the double bonds in 1,3-butadiene and their subsequent reactions. This reaction class is very important in determining the fuel reactivity at low and intermediate temperatures (600–900 K). Four possible addition reactions have been considered. (c) $^3\ddot{O}$ atom addition to the double bonds in 1,3-butadiene is very important in determining fuel reactivity at intermediate to high temperatures (> 800 K). In this reaction class, the formation of two stable molecules, namely $CH_2O +$ allene, inhibits reactivity whereas the formation of two radicals, namely $\dot{C}_2H_3$ and $\dot{C}H_2CHO$, promotes reactivity. (d) $\dot{H}$ atom addition to the double bonds in 1,3-butadiene is very important in the prediction of laminar flame speeds. The formation of ethylene and a vinyl radical promotes reactivity and it is competitive with H-atom abstraction by $\dot{H}$ atoms from 1,3-butadiene to form the resonantly stabilized $\dot{C}_4H_5$-i radical and H_2 which inhibits reactivity. *Ab initio* chemical kinetics calculations were carried out to determine the thermochemistry properties and rate constants for some of the important species and reactions involved

in the model development. The present model is a decent first model that captures most of the high-temperature IDTs and flame speeds quite well, but there is room for considerable improvement especially for the lower temperature chemistry before a robust model is developed.

1. Introduction

1,3-Butadiene is an important intermediate towards the formation of soot and poly-aromatic hydrocarbons (PAH) through the proposed "$C_2 + C_4$" benzene formation pathways. Therefore, an accurate knowledge of 1,3-butadiene oxidation chemistry is essential to the further development of models for PAH and soot formation. Moreover, 1,3-butadiene is also an important intermediate in the pyrolysis and oxidation of higher-order hydrocarbons, and its oxidation kinetics are important to the hierarchical development of the kinetic mechanisms of hydrocarbon combustion. Thus, the development and validation of combustion models for 1,3-butadiene will help improve our knowledge of detailed C_4 combustion chemistry and is an extension of our previous studies of the butene isomers [1–3].

Ignition delay times for 1,3-butadiene oxidation were previously measured by Fournet et al. [4] and Libby et al. [5]. Fournet et al. [4] measured ignition delay times for 1,3-butadiene/O_2/argon mixtures containing 85–95% argon diluent in the temperature range 1200–1700 K, at pressures of 8.5–10 atm. Libby et al. [5] measured ignition delay times in the temperature range 1390–1810 K at pressures in the range 1.5–3.8 atm at equivalence ratios from 0.25–1.0. Davis and Law [6] measured the laminar flame speeds for 1,3-butadiene/air mixtures by using the counter-flow twin flame configuration over an extensive range of equivalence ratios at standard conditions of temperature and pressure. Hansen et al. [7] used molecular-beam flame-sampling and time-of-flight mass spectrometry to measure the intermediate species to unravel important pathways leading to the formation of benzene in a pre-mixed, laminar, low-pressure 1,3-butadiene flame. They concluded that the reactions $\dot{C}_3H_3 + \dot{C}_3H_3 \leftrightarrow C_6H_6$ and $\dot{C}_4H_5\text{-}i + C_2H_2 \leftrightarrow C_6H_6 + \dot{H}$ are roughly of equal importance in benzene formation.

There is a dearth of experimental ignition delay time data available in the literature for 1,3-butadiene at lower temperatures (650–1200 K) and at higher pressures (> 10 atm), which are conditions of direct relevance to gasoline, diesel and low-temperature combustion engine technologies. Moreover, further measurements of flame speeds and species concentration profiles in reactors will also contribute to an improved understanding of 1,3-butadiene pyrolysis and oxidation. In this work, ignition delay time measurements of 1,3-butadiene oxidation under engine conditions including both low to intermediate (600–1000 K) and higher temperatures (1000–1600 K) have been measured. Additionally, flame speed measurements at 1 and 5 atm at temperatures of 295 K, 359 K and 399 K and over a wide range of equivalence ratios have also been taken.

2. Experimental methods

In this study, ignition delay times for the oxidation of 1,3-butadiene were measured at fuel-lean, stoichiometric and fuel-rich equivalence ratios with various levels of argon dilution, or in air, as was the case for one of the mixtures. Additionally, pressure ranges examined in the study spanned the range of $p_5 = 1$–40 atm, where p_5 is the reflected-shock pressure. The mixture compositions as well as the facility used for each mixture are shown in Table 1. 'Air' in the case of the experiments presented in this study refers to nitrogen and oxygen in a 79/21 ratio. The shock tube (ST) experiments were carried out in the shock tubes at Texas A&M Univer-

sity (TAMU), King Abdullah University of Science and Technology (KAUST), Xi'an Jiaotong University (XJTU), the University of Central Florida (UCF), and at NUI Galway (NUIG). All RCM experiments were carried out in the twin-opposed piston RCM at NUIG. The mixture compositions (mole %) investigated in this study from different groups are shown in Table 2. The ignition delay times reported in this study along with associated pressure and temperature conditions are available as Supplementary material.

2.1. Ignition delay time measurements

Table 3 lists the details of each shock tube and measurement techniques described in this work. Even though the measurement technique or exact definition of ignition delay time adopted by each experimental group is slightly different, the simulation results for ignition delay time are consistent with the experimental definition. This similarity is primarily due to the fact that most markers for ignition delay time are similar when the mixtures are at least reasonably exothermic ($< 96\%$ dilution).

2.1.1. NUI Galway rapid compression machine

Ignition delay times for 1,3-butadiene/'air' mixtures at $\varphi = 0.5$, 1.0 and 2.0 at pressures of approximately 10, 20 and 40 atm were measured at NUIG in the rapid compression machine which has been described in the recent propene study by Burke et al. [15]. Here the 'air' used in these experiments is a mixture of O_2 and N_2 in the molar ratio of 1:3.76. The ignition delay time definition in this work is shown in Fig. 1 and is taken from the time of peak pressure at the end of compression to the time of maximum rate of pressure rise due to ignition.

It is well known that the heat loss profiles generally garnered from experimental, nonreactive pressure profiles must be included to simulate rapid compression machine data accurately. To this end, a nonreactive profile, for which an experiment is performed by replacing oxygen with nitrogen in the fuel–"air" charge, has
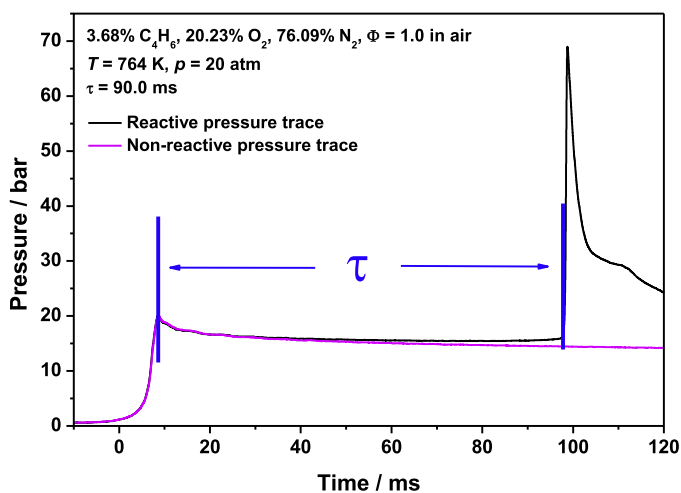

Fig. 1. Sample pressure trace from the NUI Galway RCM for 1,3-butadiene oxidation. (Pink line: nonreactive trace, black line: reactive trace). (For interpretation of the references to color in this figure legend, the reader is referred to the web version of this article.)

Table 1
Ignition delay time, flame speed, and speciation measurements for 1,3-butadiene oxidation used in model validation.

Experiment	Initial conditions		Reactant composition %				Reference
	T (K)	p (atm)	φ	1,3-C_4H_6	O_2	Bath gas	
Shock tube IDT	990–1781	1–40	0.5–2.0	1–7.1	2.8-27.5	Ar, N_2	This work
RCM IDT	645–961	10–40	0.5–2.0	1.9–7.1	20	N_2	This work
Flame speed	295–399	1-5	0.6-1.7	2.2–6.1	19.7–20.5	N_2	This work
Single-pulse shock tube	1200–1800	6.5	∞	0.175	–	99.83 (Ar)	Colket [8]
Single-pulse shock tube	1200–1800	1.4–2.2	∞	0.5	–	99.5 (Ar)	Hidaka et al. [9]
Shock tube IDT	1390–1810	1.5–3.8	0.25–1.0				Libby et al. [5]
Shock tube IDT	1200–1700	8.5–10	0.69–1.38	1.0–3.0	4.0–12.0	85–95 (Ar)	Fournet et al. [4]
Flow reactor	1100–1185	1	∞	0.3	–	99.7 (N_2)	Laskin et al. [10]
Flow reactor	1035–1125	1	0.55–1.65	0.14	0.12–1.4	98.5–99.4 (N_2)	Laskin et al. [10]
Flow reactor	1125	1	1.18–1.65	0.143	0.48–0.63	99.2–99.4 (N_2)	Brezinsky et al. [11]
Jet-stirred reactor	750–1250	1.0–10.0	0.25–2.0	0.15	0.41–3.3	96.6–99.4 (N_2)	Dagaut and Cathonnet [12]
Flame speed	–	–	0.6–1.8	–	–	–	Davis and Law [6]
Flame speciation		30 Torr	1.8	7.6	23.1	69.3 (Ar)	Hansen et al. [7]
Flame speciation		20 Torr	2.4	29.5	67.5	3.0 (Ar)	Cole et al. [13]

Table 2
Mixture compositions (mole %) investigated in this study.

φ	1,3 Butadiene	O_2	Diluent	P (atm)	Facilities
0.3	1.13	20.70	77.88 (N_2)	10, 20, 40	ST (NUIG)
0.5	1.87	20.57	77.34 (N_2)	10, 20, 40	RCM, ST (NUIG)
1.0	3.68	20.24	76.10 (N_2)	10, 20, 40	RCM, ST (NUIG)
2.0	7.10	19.53	73.414 (N_2)	10, 20, 40	RCM, ST (NUIG)
0.3	1.00	18.30	80.7 (Ar)	1	ST (UCF)
0.5	1.00	11.00	88 (Ar)	1, 2, 4	ST (TAMU&UCF)
1.0	1.00	5.50	93.5 (Ar)	1, 2, 4	ST (TAMU&KAUST)
1.0	5.00	27.50	67.5 (Ar)	1	ST (KAUST)
2.0	1.00	2.75	96.25 (Ar)	1, 2, 4	ST (KAUST&XJTU)

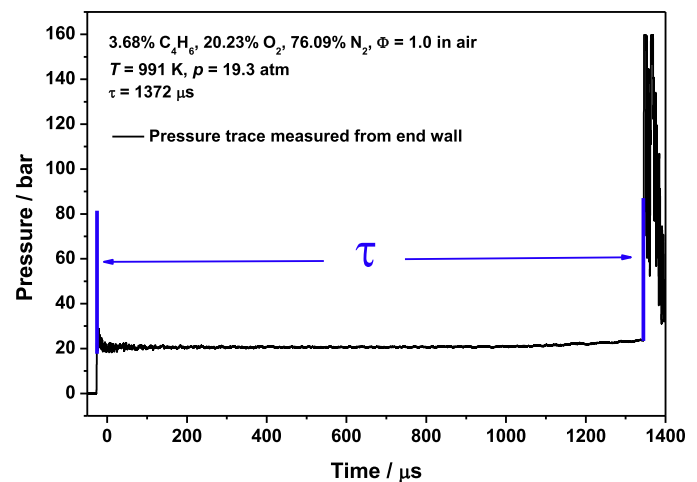**Fig. 2.** Sample pressure trace from NUI Galway ST for 1,3-butadiene oxidation.

been measured for each mixture and compared with the reactive profile as shown in Fig. 1. The volume history used for the simulation includes the heat loss during the compression stroke by adding an empirically determined additional volume, and the pressure drop, primarily due to heat loss after the end of compression, was accounted for by the "adiabatic core expansion" approach. The volume history is then used as an input in the Chemkin input file. Detailed discussion about the heat loss and its simulation can be found in the previous studies [19,20].

2.1.2. NUI Galway (NUIG) high-pressure shock tube

Ignition delay times for 1,3-butadiene oxidation were measured in the high-pressure shock tube at NUIG, which has already been described in detail by Burke et al. [15]. Ignition delay times were recorded for 1,3-butadiene/'air' mixtures at $\varphi = 0.5$, 1.0 and 2.0 at pressures of approximately 10, 20 and 40 atm in the temperature range of approximately 950–1350 K. The ignition delay time was defined as the time interval between the rise in pressure due to the arrival of the reflected shock wave at the endwall and the maximum rate of rise of the pressure signal, as shown in Fig. 2.

2.1.3. Texas A&M University (TAMU) shock tube

The shock-tube facility used in this work is described in Aul et al. [16]. Gas mixtures were made using the partial pressure method, where the mole fractions of each species were known

within ± 1% uncertainty. The mixtures used in this study were considered somewhat dilute but were not what is traditionally considered to be dilute (98% Ar and above, by volume). Thus, both endwall and sidewall diagnostics were of use in verifying accurate interpretations of ignition delay times, with the endwall diagnostics being the primary data collection methods. An example time-history plot of pressure and emission traces for an ignition delay time experiment in this study is shown in Fig. 3. When non-dilute mixtures are investigated, the endwall pressure trace is an acceptable means of determining both time zero and the onset of ignition and is aided by the use of an endwall emission diagnostic. This use of pressure rise for ignition was shown to be a good assumption while conducting this study. However, sidewall pressure and emission diagnostics, respectively, were also used to aid in verifying ignition delay time and the detection of OH* in the case of a weaker pressure rise at ignition due to Ar dilution.
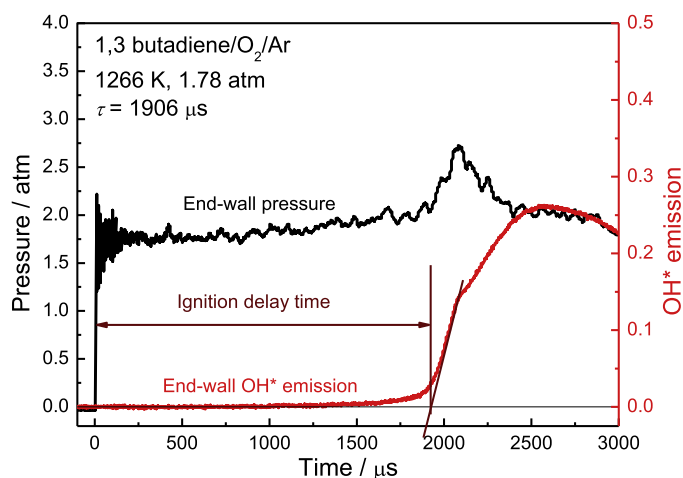
Table 3
Facility information summary for different group used in this study.

ST	Diameter (cm)	Diaphragm	Side-wall ignition	End-wall ignition	dp/dt (%/ms)	1,3-butadiene purity	Ref.
KAUST	14	Polycarbonate	Pressure, OH*	N/A	3.5%	≥99%	[14]
NUIG	6.35	Aluminum	N/A	Pressure	3–10%	≥99%	[15]
TAMU	15.24	Polycarbonate	Pressure, OH*	Pressure, OH*	1–2%	99.50%	[16]
XJTU	11.5	Polyethylene terephthalate	N/A	Pressure and OH*	4%	99.50%	[17]
UCF	14.17	Polycarbonate lexan	Pressure, OH*, $X_{1,3\text{-butadiene}}$	N/A	0–9%	≥99%)	[18]
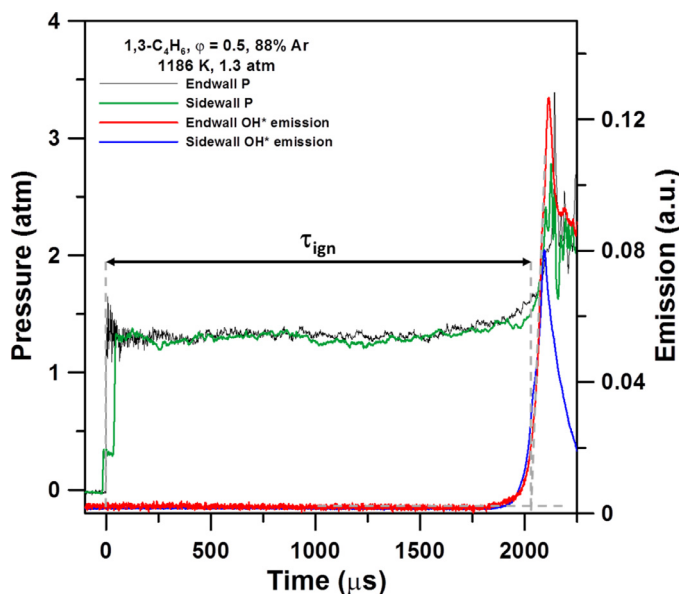
Fig. 3. Sample time history traces of experimental data from endwall and sidewall pressure transducers from the TAMU shock tube, as well as endwall and sidewall emission diagnostics for OH* chemiluminescence. Experimental conditions 1.0% 1,3-C_4H_6, $\varphi = 1$, 93.5% Ar, 1.16 atm, 1476 K.
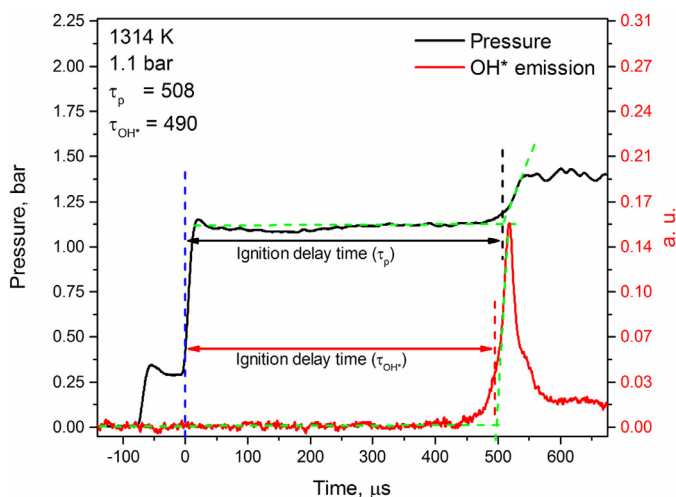

Fig. 4. A representative ignition delay time measurement from OH* and pressure profiles from the KAUST shock tube. Test mixture composition: 1% 1,3-C_4H_6 / 5.5% O_2/ 93.5% Ar.
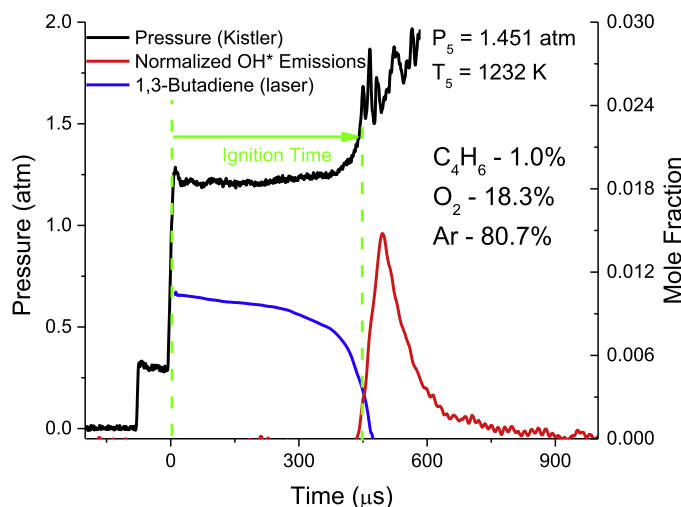
2.1.4. King Abdullah University of Science and Technology (KAUST) shock tube

The low-pressure shock tube (LPST) at KAUST (details in [14]) was used to measure the ignition delay times of 1,3-butadiene/O_2/Ar mixtures at pressures of 1, 2 and 4 bar, equivalence ratios of 1 and 2, and temperatures ranging from 1060 to 1675 K. The ignition delay time is defined as the period of time from the arrival of the reflected shock wave to the onset of ignition. The pressure trace and the OH* emission, detected at the sidewall, were used to determine the onset of ignition. Figure 4 shows an example of ignition delay time measurement from the OH* and pressure profiles.

2.1.5. Xi'an Jiaotong University (XJTU) shock tube

Measurements of ignition delay times for 1, 3 butadiene/O_2/Ar mixtures at 1.0, 2.0 and 4.0 atm at $\varphi = 2.0$, and at 1.0 atm at $\varphi = 0.3$ were performed in the XJTU stainless-steel shock tube

Fig. 5. Example 1,3-butadiene ignition delay time measurement from XJTU shock tube.

(details in [17]). The mixture components used in this study were 1, 3 butadiene (99.5%), O_2 (> 99.99%), Ar (> 99.99%) and He (99.999%). Ignition delay time determination was made behind reflected shock waves by measuring the pressure and OH* emission at the endwall of the driven section (see Fig. 5). During the measurements, an obvious pressure rise ($dp/dt = 4\%/ms$) resulting from non-ideal facility effects was observed before the main ignition event, and this effect has been taken into consideration for the simulation when ignition delay time is longer than 1.5 ms.

2.1.6. University of Central Florida (UCF) shock tube

Experiments were performed in a stainless-steel shock tube of 14.17 cm inner diameter located at UCF as described in Loparo et al. [18]. The data presented were taken at a sidewall location 2 cm away from the endwall of the driven section using pressure and OH* emission. Research grade (from Praxair Inc.) argon (99.999%), oxygen (99.999%) nitrogen (99.999%), and 1,3-butadiene ($\geq$ 99%) (from Fisher Sci.) were used to prepare mixtures of 1,3-butadiene/oxygen diluted in Ar/N_2 at equivalence ratios (φ) ranging from 0.3 to 0.5 and initial 1,3-butadiene mole fractions between 0.01 and 0.0113. In addition, a tunable CO_2 gas laser (Access Laser L4GS), tuned to the P14 line at 10.532 μm, was used for measuring 1,3-butadiene time-histories via a direct absorption spectroscopy scheme (details of the laser measurements in [18]). Example pressure, OH* and 1,3-butadiene time-histories from the reflected shock is shown in Fig. 6. The onset of ignition was determined by four methods: finding the time of steepest rise of the OH* emission and pressure, then linearly extrapolating back in time to the pre-ignition baseline, time for 1/3rd decay of initial butadiene concentration, and from the time of maximum OH* emission.

The ignition delay times measured via the end-wall and side-wall can be different from each other. However, these differences are usually found to be quite small (~10%) when the mixtures are at least reasonably exothermic (dilution < 96%). At very high temperatures and for exothermic mixtures, ignition occurs very close to the end-wall and can send a detonation-like strong ignition wave towards the side-wall and thus artificially expediting the observed ignition at the side-wall. If the side-wall is located very close to the end-wall, the difference between the two measurements will be small, such that the whole region near the endwall of the shock tube will seemingly ignite at the same time within the resolution of the diagnostics. Therefore, in such situations, an end-wall diagnostic is more reliable. At conditions that are highly diluted (i.e., little to no energy release), side-wall ignition

Fig. 6. Pressure time-history in the test Section 2 cm from the endwall of UCF shock tube for an experiment using 1% 1,3-C$_4$H$_6$ in Ar at $\varphi = 0.3$, $T_5 = 1232$ K, $p_5 = 1.451$ atm.

Fig. 7. Sample flame speed images of 1,3-butadiene-air at (a) 358 K, 1 atm and (b) 358 K, 5 atm.

diagnostic is better due to a more-resolved temporal/spatial resolution. The temperature behind reflected shock waves was calculated using measured shock velocity and shock-jump relations. Generally, the uncertainty in T_5 is < 1% and comes primarily from the uncertainty in measured shock velocity and thermodynamic parameters. The uncertainty in T_5 is included in the estimation of the overall uncertainty in ignition delay time measurements, which is generally between 20% and 25%.

2.2. Laminar flame speed measurements (TAMU)

Laminar flame speed experiments were performed at Texas A&M University in the high-temperature, high-pressure (HTHP) laminar flame speed vessel. This vessel is a spherically expanding flame experiment capable of initial pressures of up to 10 atm and temperatures ranging from room temperature to 475 K. For initial temperatures above room temperature, the vessel is heated using a heating jacket. The fill and exhaust lines are heated by using heating tape, controlled to within 1 °C, and insulation. The vessel has been previously checked for temperature uniformity with an array of thermocouples, which also agreed to within 1 °C. Mixtures were made inside the HTHP vessel using the partial pressure method. When appropriate, the components were measured either using a 0–1000 Torr (0–133 kPa) or 0–500 psi (0–3.45 MPa) pressure transducer with uncertainties of ± 0.1 Torr (13 Pa) and ± 0.1 psi (0.69 kPa), respectively. The ignition event was initiated with a spark between two sharpened steel rods, and the high voltages required were generated by an automotive ignition coil. Finally, images of the propagating flame were obtained using a Z-type schlieren setup to enhance the density gradients for capture with a high-speed camera. This Z-type setup has been modified with flat mirrors to minimize angles that might cause image aberrations. Example images from this study are shown in Fig. 7. These images were then used as the basis for the analysis procedure. For more details on the experimental setup, see de Vries et al. [21] and Lowry et al. [22].

The data processing takes the digital flame propagation frames and uses a custom MATLAB routine to best fit a circle to the flame edge of each frame to determine its radius. With the flame radii and the frame rate of the camera, another MATLAB routine uses established nonlinear stretch correction techniques [23–27] to extrapolate the burned, stretched flame speed data to the burned, un-stretched flame speed, $S_{L,b}^0$. For these experiments, special care
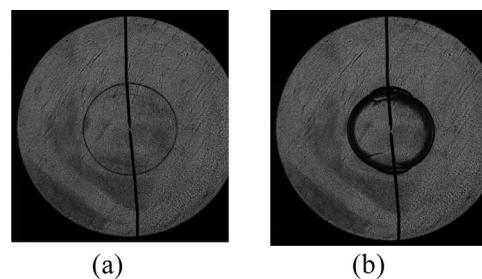
was taken to ensure the data used for the fit were unaffected by ignition, confinement, and instability acceleration. The resulting $S_{L,b}^0$ is converted to its unburned, un-stretched flame speed value by multiplying it by the appropriate density ratio, $S_L^0 = (\rho_b/\rho_u)S_{L,b}^0$. The burned- and unburned-gas densities used for the density ratio are obtained using thermochemistry at experimental conditions using an adiabatic flame calculation.

3. Computational method

In this work, rate constants for important reactions and the thermochemistry of important species have been assigned based on electronic structure calculations for reactions combined with statistical rate theory. The compound electronic structure methods CBS-QB3 [28,29], G3 [30], and G4 [31] have also been used to calculate the thermochemistry of important species for comparison. The heat of formation of 1,3-butadiene at 298 K used in this study was calculated to be 26.68 kcal mol^{-1} (quantum chemistry calculations) and 26.0 kcal mol^{-1} (group additivity [32]) which are both similar to the experimental result of 26.01 kcal mol^{-1} from Prosen et al. [33] and the calculated result of 26.5 kcal mol^{-1} from Goldsmith et al. [34]. The entropy of 1,3-butadiene at 298 K used here is 66.60 cal K^{-1} mol^{-1} (*ab initio* calculations in this work) and 66.56 cal K^{-1} mol^{-1} (group additivity in this work) which are close to the calculation result of 65.8 cal K^{-1} mol^{-1} from Goldsmith et al. [34]. The heat of formation of 1,3-cyclopentadiene at 298 K used here was calculated to be 32.1 kcal mol^{-1} (group additivity) which is similar to the experimental result of 31.9 kcal mol^{-1} from Furuyama et al. [35]. The group additivity method has been used to calculate the thermochemistry properties for all of the other species relevant to the 1,3-butadiene sub-mechanism.

Oxygen atom addition to 1,3-butadiene is crucially important in predicting 1,3-butadiene reactivity at temperatures of 1000 K and above. A comprehensive analysis of the detailed mechanism of Ö + 1,3-butadiene is complicated by the existence of many possible channels and inter-system crossing between triplet and singlet potential energy surfaces. Comprehensive potential energy surfaces for both ^{3}Ö and ^{1}Ö reacting with 1,3-butadiene have been investigated in this work along with the inter-system crossing reactions between these two potentials, however the rate constants for these reaction channels are still under investigation. The details of this computational method will be discussed in a separate theoretical paper for this reaction system, however a summary of these computational methods is provided here. Geometry and frequency calculations for reactants, transition states, intermediates and products were carried out at the UWB97XD [36] level of theory using the aug-cc-pVTZ [37] basis set. Single point energy calculations were carried out at the UCCSD(T)/aug-cc-pVTZ level of theory with basis set corrections from MP2/aug-cc-pVQZ and MP2/aug-cc-pVTZ. For species containing a highly multi-reference character, the single point energy was obtained at the CASPT2 [38,39] level using the aug-cc-pVTZ basis set with six active electrons and six
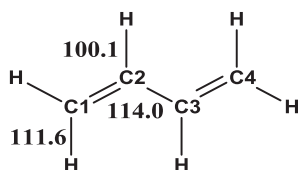
Fig. 8. Bond dissociation energy (in kcal mol^{-1}) for different bonds in 1,3-butadiene obtained at QCISD(T)/CBS//M062x/6-311++G(d,p) level of theory at 0 K.

(a) ΔH_f (298 K) = 83.4 kcal/mol   (b) ΔH_f (298 K) = 75.4 kcal/mol

Fig. 9. (a) Vinylic and (b) allenic resonance structures of the $\dot{C}_4H_5$-i radical obtained at the G4 level of theory.

active spaces. The kinetics over the reaction potential energy surface was studied by integrating the master equation using RRKM micro-canonical rate constants. RRKM rates $k(E,J)$ were determined as a function of energy E and angular momentum J using density of states convoluted over all external rotational and vibrational degrees of freedom.

Hydrogen atom addition to 1,3-butadiene and its subsequent decomposition reactions are also very important in determining the reactivity of 1,3-butadiene at 1000 K and higher temperatures. We have carried out the *ab initio* calculations to describe the detailed reaction kinetics of hydrogen addition [40]. Rate constants from the computation have been adopted in this model.

4. Model development

The current mechanism development is based on a series of previous studies which include the H$_2$/O$_2$ sub-mechanism of Kéromnès et al. [41], the C1–C2 sub-mechanism from Metcalfe and co-workers [42], the propene/allene/propyne sub-mechanism from Burke et al.[15,43], the CH$_4$/DME sub-mechanism from Burke et al. [44], the isobutene sub-mechanism development by Zhou et al. [1] and the 1- and 2-butene sub-mechanism developed by Li et al.[2,3]. Key reactions for 1,3-butadiene oxidation at different temperature and pressure conditions were highlighted by performing brute force sensitivity analyses of ignition delay times, flux analyses and flame speed sensitivity analyses and a detailed chemical kinetic mechanism (AramcoMech 3.0) has been developed. The 1,3-butadiene combustion chemistry model developed in this work has improved the predictions against a variety of experimental results. The important reactions identified by performing these kinetic analyses are discussed below.

In addition to the updates described above, updates arising from the recent publication of Goldsmith et al. [45] have been included in our model. The ongoing and simultaneous development of the overall AramcoMech model within Galway have meant that the incorporation of the theoretical calculations for the reactions described in full in [45] have been adopted without alteration as part of this release of the model. The reactions updated are all part of the generally well known low-temperature reaction scheme describing the oxidation of alkanes. In order to further improve predictions of the current model and propane ignition delay times the H-atom abstraction from propane by hydroxyl radicals have also been updated to the values measured by Sivaramakrishnan and Michael [46]. A minor increase of 30% to the rate constant for abstraction from the secondary site has been applied in order to optimize the model predictions. These changes do not represent the focus of the current work but are a result of the continual development of the overall AramcoMech model, in order to reflect the most up to date kinetic data where possible.

4.1. Geometry of 1,3-butadiene and important radicals

Bond dissociation energies (BDEs) for different bonds in 1,3-butadiene are shown in Fig. 8. It can be seen the vinylic-allylic-C2–H bond has a lower BDE (100.1 kcal mol^{-1}) than the secondary vinylic C–H bond in propene which is 106.33 kcal mol^{-1},

and which is also much higher than the BDE for the allylic C–H bond (86.4 kcal mol^{-1}) in propene [1]. This interesting comparison shows that the property of the vinylic-allylic C–H bond in 1,3-butadiene lies between the secondary vinylic C–H bond and the allylic C–H bond.

One important radical formed during the pyrolysis/oxidation of 1,3-butadiene is C$_4$H$_5$-i, which has two resonantly stabilized vinylic and allenic structures, Fig. 9. Heat of formation calculations show that the allenic structure is about 7.92 kcal mol^{-1} lower than the vinylic one and thus the allenic structure is predicted to be the dominant one.

4.2. Sensitivity analyses highlighting important reaction classes

Brute force sensitivity analyses were carried out in order to identify the key reactions which control the fuel's reactivity. The analyses were performed by increasing and decreasing each reaction rate expression by a factor of two and calculating the effect on the predicted ignition delay time.

The sensitivity coefficient is defined as: $S = \frac{\ln(\tau_+/\tau_-)}{\ln(k_+/k_-)} = \frac{\ln(\tau_+/\tau_-)}{\ln(2.0/0.5)}$, where, τ_+ is the ignition delay time calculated with the increased rate constant and τ_- is the ignition delay time calculated using the decreased rate constant. A positive sensitivity coefficient indicates an inhibiting reactivity while a negative sensitivity coefficient indicates a reaction promoting reactivity. Brute-force sensitivity analyses for ignition delay time were performed for 1,3-butadiene oxidation at pressure of 20 atm, and at $\varphi = 0.5$ in air at temperatures ranging from 770 to 1500 K, Fig. 10. Detailed discussions of the important reactions at different temperatures are provided in the next section together with the model development to identify the important reaction classes at different temperatures.

4.3. Important reactions at low temperature

In this study, we consider low temperatures to range from 600 to 1000 K and high temperatures to range from 1000 K and higher.

4.3.1. 1,3-C$_4$H$_6$+ȮH addition reaction and their subsequent reactions

At the lower temperature of 770 K, ȮH radical addition to the C=C double bonds and the subsequent reactions of the radicals formed play a very important role in predicting fuel reactivity, Fig. 10. Figure 11 shows the important reaction pathways below 870 K, with the reactions highlighted in red promoting reactivity and those in blue inhibiting reactivity. Two main products can be formed through terminal and central addition of ȮH radicals to the double bond. No experimental or theoretical investigations are available in the literature for these reactions. In our model we use rate constants analogous to ȮH radical additions to propene from Zádor et al. [47]. We realize that this analogy may introduce a large uncertainty as the carbon type in 1,3-butadiene and also the product property is quite different from that of the propene system. Future experimental measurements and/or theoretical calculations for this reaction would be helpful in determining the low temperature chemistry of 1,3-butadiene. We also find that the reaction involving ȮH radical terminal additions forming the resonantly-stabilized alcohol radicals (C$_4$H$_6$4,2-1OH) inhibit reactivity, while ȮH radical additions to the central carbon atom
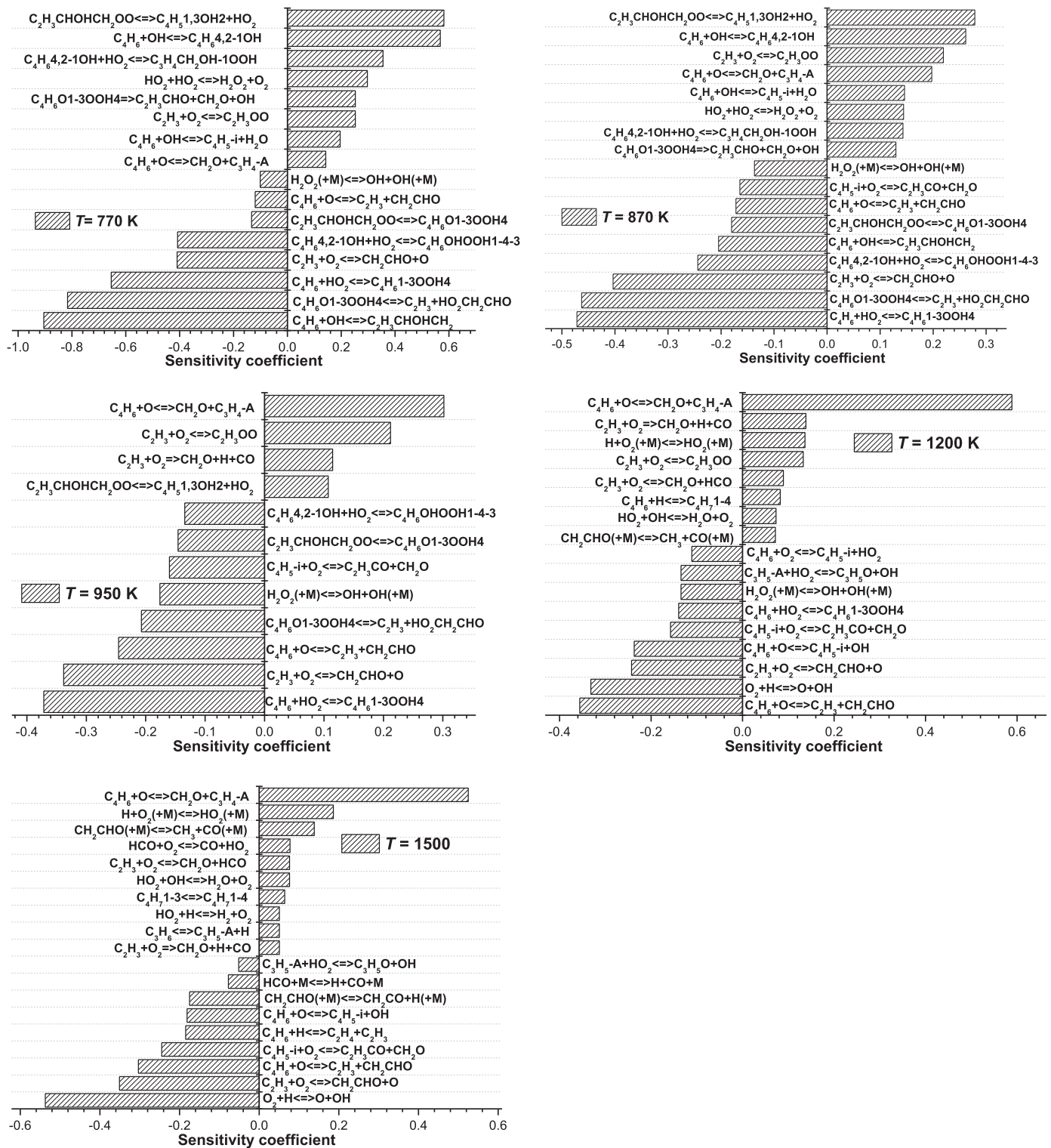
Fig. 10. Brute-force sensitivity analysis of 1,3-butadiene ignition delay times at 20 atm, $\varphi = 0.5$ for temperatures from 770 K to 1500 K.

forming the alcoholic alkene radical ($C_2H_3CHOHCH_2$) promotes reactivity.

The resonantly stabilized alcohol radicals ($C_4H_64,2$-1OH) formed mainly react with $H\dot{O}_2$ radicals through radical-radical recombination reactions. Two products are obtained through terminal and central additions to form $C_3H_4CH_2OH$-1OOH (inhibiting) and $C_4H_6OHOOH1$-4-3 (promoting), Fig. 11. Both of these species decompose through O–O bond breaking followed by β-scission

reactions which are not discussed in detail here. Rate constants for the recombination reactions are taken by analogy with the calculations provided by Goldsmith et al. [48] for allyl + $H\dot{O}_2$ radicals. This treatment also introduces an uncertainty for the model because there is no alcohol group influence in the allyl + $H\dot{O}_2$ reaction system while in this system the influence of the alcohol group should have an impact on the rate constant. Future theoretical investigations on this reaction class will also be very important in
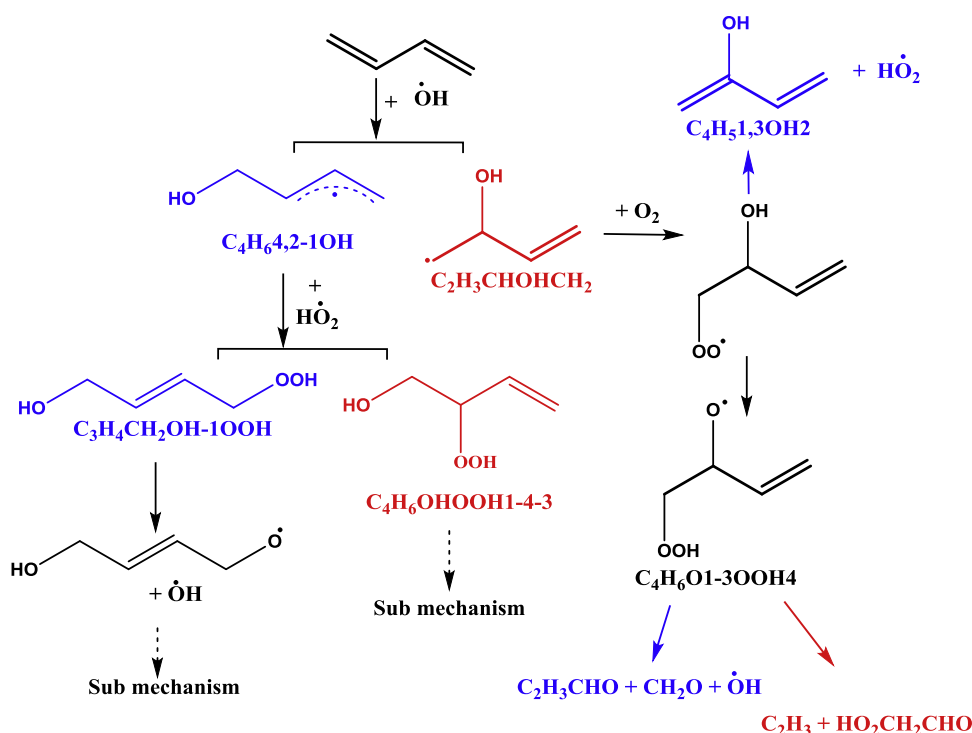
Fig. 11. Important reaction channels for $1,3\text{-}C_4H_6 + \dot{O}H$ addition reaction and their subsequent reactions. Formation of the species highlighted in red: promote reactivity, in blue: inhibit reactivity. (For interpretation of the references to color in this figure legend, the reader is referred to the web version of this article.)

producing accurate predictions of the low temperature oxidation of 1,3-butadiene.

The products of $\dot{O}H$ radical addition to the central carbon atom in 1,3-butadiene can react with molecular oxygen to form alcohol $R\dot{O}_2$ species such as $C_2H_3CHOHCH_2O\dot{O}$ radicals, Fig. 11. Rate constants for these reactions are also based on analogy with alkyl radical addition to O_2 calculated by Miyoshi [49]. This treatment also introduces uncertainty to our model because there is no alcohol group influence in allyl radicals while the influence of the alcohol group should influence the rate constant. Five isomerization reaction pathways have been taken into consideration for the formed alcoholic $R\dot{O}_2$ radical of $C_2H_3CHOHCH_2O\dot{O}$ and only two of the reaction channels show sensitivity to the fuel reactivity. Namely, the $H\dot{O}_2$ elimination reaction inhibits the fuel reactivity along with the six membered-ring isomerization reaction that forms $C_4H_6O1\text{-}3OOH4$, Fig. 11.

4.3.2. $1,3\text{-}C_4H_6 + H\dot{O}_2$ addition reaction

Four reaction channels have been considered for the addition of $H\dot{O}_2$ radicals with 1,3-butadiene, Fig. 12. $H\dot{O}_2$ radicals can add directly to the terminal (channel 1) or central (channel 3) carbon atom in 1,3-butadiene, leading to the first two channels. Moreover, the O–H bond in the $H\dot{O}_2$ radical can also break when the O–O in the $H\dot{O}_2$ radical adds to the terminal carbon (channel 2) and/or the central carbon atom (channel 4). Rate constants for these reactions have not been either experimentally or theoretically investigated, and here we use the rate constants calculated by Villano et al. [50] for the addition of $H\dot{O}_2$ radicals to butene molecules by analogy. This also introduces uncertainty for the model predictions as the carbon type in olefins and dienes are somewhat different.

For channel 1, the $H\dot{O}_2$ radical adds to the terminal carbon of $1,3\text{-}C_4H_6$ directly to form a resonantly stabilized hydroperoxyl-alkyl ($\dot{Q}OOH$) radical ($C_4H_61\text{-}3OOH4$). For this type of radical, its recombination reaction with $H\dot{O}_2$ radical is dominant at low and intermediate temperatures. Two products are formed through recombination with the terminal carbon atom ($C_4H_62\text{-}OOH14$) or central

carbon atom ($C_4H_61\text{-}OOH34$). Both of these species can decompose through O–O bond cleavage followed by β-scission reactions, Fig. 12. The decomposition of the terminal carbon adducts $C_4H_62\text{-}OOH14$ does not influence the fuel reactivity, whereas decomposition of the central carbon adducts $C_4H_61\text{-}OOH34$ has a significant influence on the fuel reactivity, Fig. 10. The formation of vinyl radicals and the HO_2CH_2CHO species significantly promotes reactivity while the formation of $C_2H_3CHO + CH_2O + \dot{O}H$ inhibits reactivity. The branching ratio between these two reaction channels is also important in determining the final reactivity of 1,3-butadiene oxidation at low temperatures. Rate constants for those reaction channels are also taken by analogy with the reaction of allyl with $H\dot{O}_2$ radicals as calculated by Goldsmith et al. [48].

For channel 2, where the $H\dot{O}_2$ radical adds to the terminal carbon, the O–H bond breaks and the OO group adds to the terminal carbon and the $\dot{H}$ atom adds to the central carbon. A five-membered ring structure is formed in the transition state. The adduct will mainly isomerize to $C_4H_61\text{-}3OOH4$ through a five-membered transition state involving a H-atom transfer.

For channel 3, $H\dot{O}_2$ radical adds to the central carbon of $1,3\text{-}C_4H_6$ directly to form an alkenyl QOOH radical ($C_4H_61\text{-}4OOH3$). This adduct can form a cyclic ether $+ \dot{O}H$ radical or it can add to molecular oxygen to form an alkenyl $\dot{O}_2QOOH$ radical. This $\dot{O}_2QOOH$ radical can be consumed through isomerization and subsequent β-scission reactions, Fig. 12. Rate constants for these reaction processes are taken by analogy with alkyl radical reactions calculated by Miyoshi [49] and Sharma et al. [51]. Channel 4 is similar to channel 3 in which the OO group adds to the central carbon and the $\dot{H}$ atom adds to the terminal carbon. The adduct mainly isomerizes to $C_4H_61\text{-}4OOH3$ through a five-membered transition state involving a H-atom transfer.

4.3.3. $\dot{C}_4H_5\text{-}i$ radical chemistry

Considering the bond dissociation energies in 1,3-butadiene, Fig. 8, it can be observed that the vinylic-allylic hydrogen bond is $11.5\,\text{kcal}\,\text{mol}^{-1}$ lower than the vinylic hydrogen bond. Hydrogen-
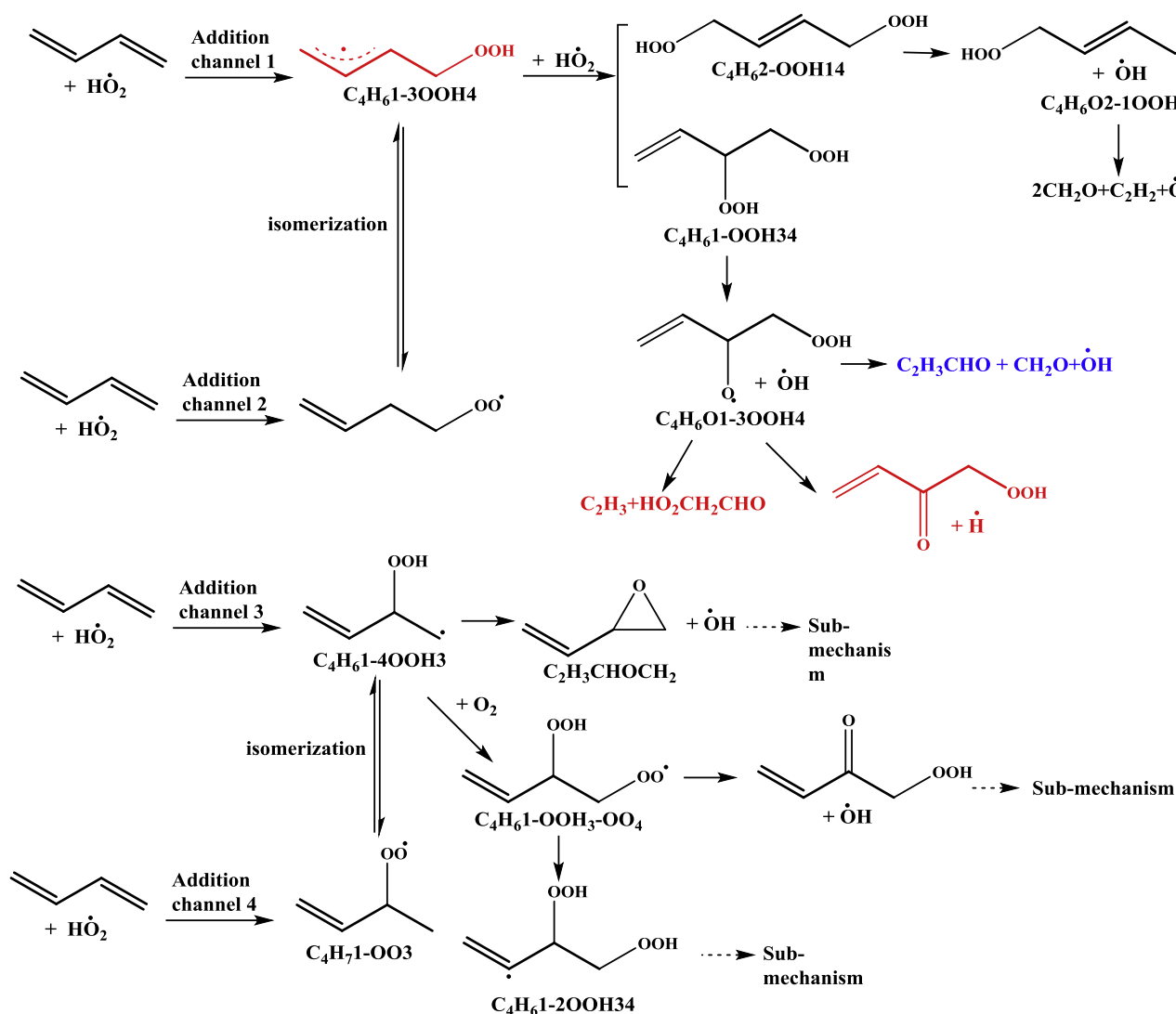
Fig. 12. Important reaction channels for the addition reaction1,3-C_4H_6 + $H\dot{O}_2$ and the subsequent reactions. Formation of the species highlighted in red: promote reactivity, in blue: inhibit reactivity. (For interpretation of the references to color in this figure legend, the reader is referred to the web version of this article.)

atom abstraction reactions by $\dot{O}H$ radical from C_2 or C_3 are the main abstraction channels leading to the formation of the resonantly stabilized allenic $\dot{C}_4H_5$-i radical, Fig. 9. The rate constants for these reactions are taken from the experimental measurements carried out by Vasu et al. [52]. The $\dot{C}_4H_5$-i radical so formed can either add to $H\dot{O}_2$ radicals or with molecular oxygen. Sensitivity analyses and flux analyses show that the $\dot{C}_4H_5$-i radicals are consumed mainly by reacting with molecular oxygen. Theoretical calculations for this reaction carried out by Rutz et al. [53] have been used in this work. The formation of vinyl radical, formaldehyde and CO is the main product channel that promotes fuel reactivity and becomes increasingly important with increasing temperature, Fig. 10.

4.4. Important reactions at high temperature

4.4.1. 1,3-C_4H_6+$\ddot{O}$ addition reactions

This reaction class is also important at low temperatures and becomes increasingly significant with increasing temperature. At 1200 K, the branching ratio between the two main product channels, namely $\dot{C}_2H_3$ + $\dot{C}H_2CHO$ or CH_2O + C_3H_4-a determines the fuel's reactivity. The important reaction pathways for this reaction are shown below. The reaction leading to the formation of the two
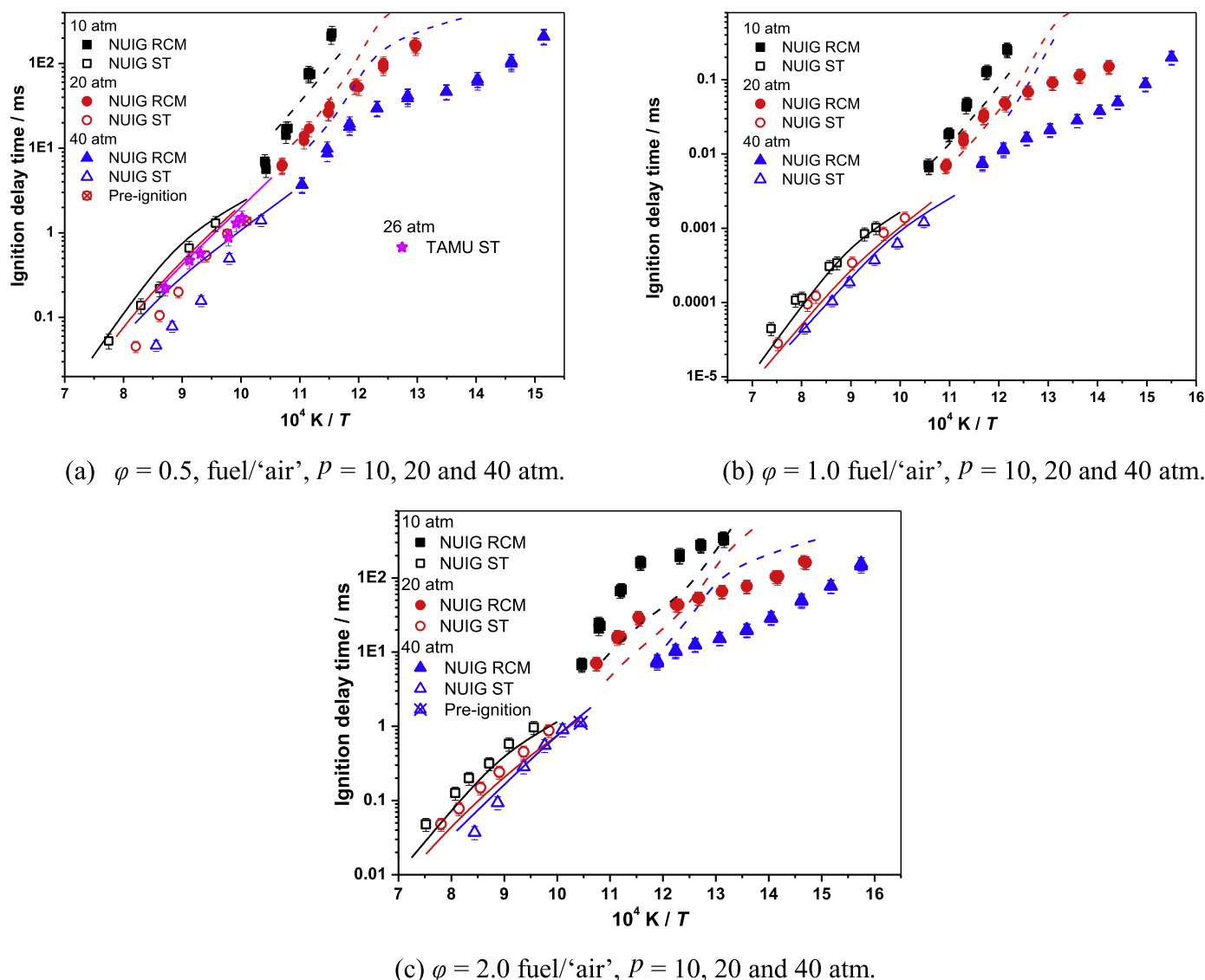
reactive radicals $\dot{C}_2H_3$ and $\dot{C}H_2CHO$ is the most promoting while that leading to the formation of the two stable molecules CH_2O and C_3H_4-a is the most inhibiting reaction channel at a temperature of 1000 K and higher, Fig. 10.

- 1,3-C_4H_6 + $\ddot{O}$ ↔ CH_2O + C_3H_4-a
- 1,3-C_4H_6 + $\ddot{O}$ ↔ $\dot{C}_2H_3$ + $\dot{C}H_2CHO$
- 1,3-C_4H_6 + $\ddot{O}$ ↔ CH_2CHCHO + $\dot{H}$

Rate constants for this reaction are taken by analogy with those for propene + $\ddot{O}$ calculated by Cavallotti et al. [54]. Theoretical calculations on the kinetics of this reaction are underway by our research group. High-level *ab initio* electronic structure calculations of underlying triplet/singlet potential energy surface and statistical (RRKM/Master Equation) computations of branching ratios including inter-system crossing calculations are being performed.

4.4.2. 1,3-C_4H_6+$\dot{H}$ addition reactions

Hydrogen atom addition to 1,3-butadiene is very important in the accurate prediction of ignition delay times at high temperatures (> 1000 K) and also the flame speeds. The important reaction channels are shown below. Rate constants for these reaction channels were calculated using RRKM theory based on the potential

(a) $\varphi = 0.5$, fuel/'air', $P = 10$, 20 and 40 atm.

(b) $\varphi = 1.0$ fuel/'air', $P = 10$, 20 and 40 atm.

(c) $\varphi = 2.0$ fuel/'air', $P = 10$, 20 and 40 atm.

Fig. 13. Influence of pressure on 1,3-butadiene ignition delay times from shock tube and RCMs for fuel/'air' mixtures. Symbols: experimental data; solid lines: constant volume simulation, dashed lines: heat loss facilities effect.

energy surface obtained at the ROCCSD(T)/cc-pV∞Z//M062X/6-311++G(d,p) level of theory [40].

- $1,3\text{-}C_4H_6 + \dot{H} \leftrightarrow \dot{C}_4H_7 1\text{-}3$
- $1,3\text{-}C_4H_6 + \dot{H} \leftrightarrow C_2H_4 + \dot{C}_2H_3$
- $1,3\text{-}C_4H_6 + \dot{H} \leftrightarrow C_3H_4\text{-}a + \dot{C}H_3$
- $1,3\text{-}C_4H_6 + \dot{H} \leftrightarrow C_3H_4\text{-}p + \dot{C}H_3$
- $1,3\text{-}C_4H_6 + \dot{H} \leftrightarrow 1,2\text{-}C_4H_6 + \dot{H}$
- $1,3\text{-}C_4H_6 + \dot{H} \leftrightarrow 1\text{-}C_4H_6 + \dot{H}$

The first two channels are the most important and are competitive; where forming the resonantly stabilized radical $\dot{C}_4H_7$1-3 inhibits reactivity while that forming reactive vinyl radicals and ethylene promotes reactivity.

4.4.3. 1,3-C$_4$H$_6$ unimolecular decomposition reactions

$1,3\text{-}C_4H_6 + M \leftrightarrow \dot{C}H_3 + \dot{C}_3H_3 + M$
$1,3\text{-}C_4H_6 + M \leftrightarrow 2\dot{C}_2H_3 + M$
$1,3\text{-}C_4H_6 + M \leftrightarrow C_2H_2 + C_2H_4 + M$
$1,3\text{-}C_4H_6 + M \leftrightarrow 2\text{-}C_4H_6 + M$
$1,3\text{-}C_4H_6 + M \leftrightarrow C_2H_2 + \dot{C}_2H_3 + \dot{H} + M$
$1,3\text{-}C_4H_6 + M \leftrightarrow C_4H_4 + \dot{H} + \dot{H} + M$

Tranter and co-workers [55] have measured the rate constants for the thermal decomposition of 1,3-butadiene in a diaphragm-less shock tube at post shock total pressures of 26–261 Torr and temperatures ranging from 1428–2354 K, using laser schlieren densitometry. Their experimental work was complemented by high-level *ab initio* calculations, which shows that the formally direct dissociation pathway to $\dot{C}H_3 + \dot{C}_3H_3$ is the dominant product channel at temperatures ranging from 1739–2354 K, with branching fractions ranging from 0.62–0.78 with greatest yields at the lowest temperatures, independent of pressure. Molecular fragmentation of 1,3-butadiene to $C_2H_2 + C_2H_4$ is a relatively minor loss channel with branching ratios ranging from 0.04–0.15, independent of pressure. The isomerization from 1,3-butadiene to 2-butyne is the most significant isomerization channel with a branching ratio of 0.12 independent of temperature and pressure. Moreover, the channels leading to direct H-atom eliminations and the formation of vinyl radicals are negligible.

5. Model validation

The developed model has been validated against a wide range of experimental measurements that have been taken during the
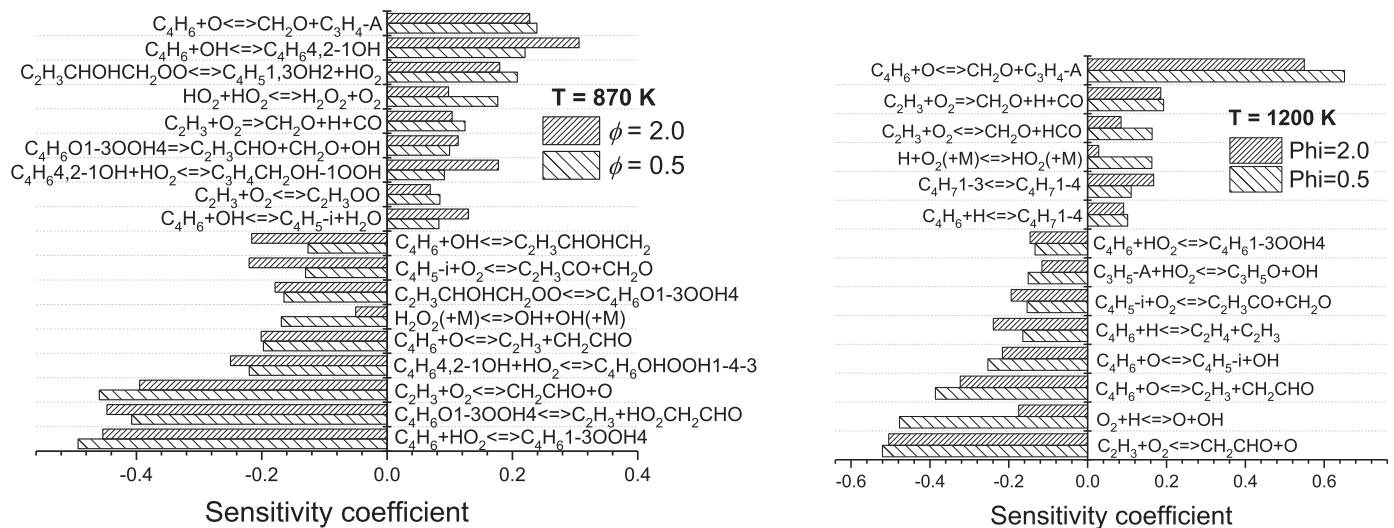
Fig. 14. Brute-force sensitivity analysis of 1,3-butadiene ignition delay times at 10 atm, $\varphi = 0.5$ and 2.0 for temperatures of 870 K and 1200 K.
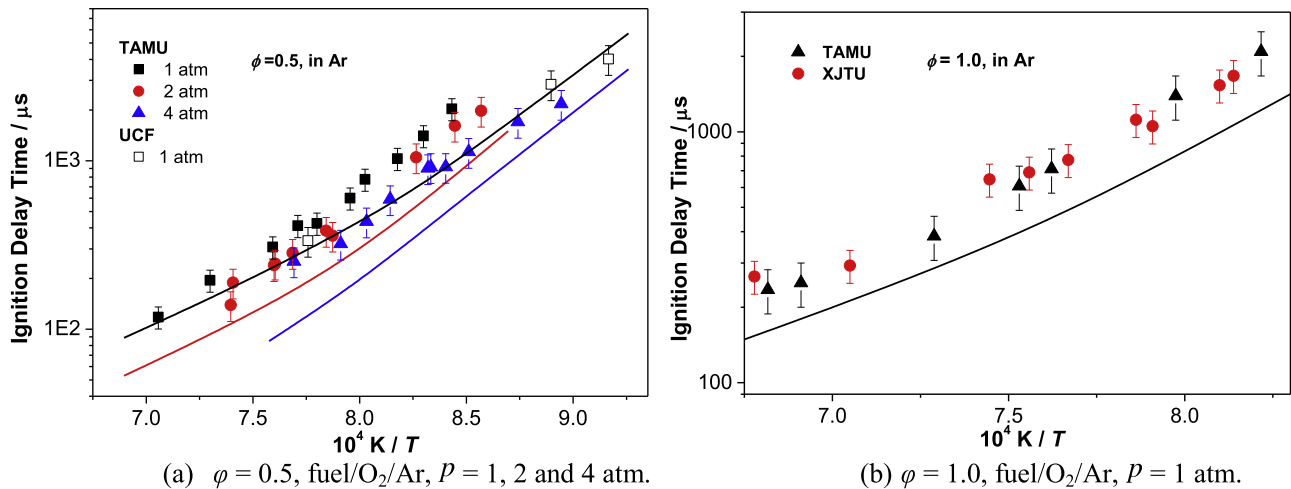

Fig. 15. Ignition delay time measurements and constant volume simulations (solid lines) for $\varphi = 0.5$ and $\varphi = 1.0$, fuel/O$_2$/Ar mixtures at different pressures. Experimental measurements from TAMU (solid symbols) and UCF (open symbols).

course of this work which cover low- and high-temperature ignition delay times (Figs. 13–18) and laminar flame speeds (Fig. 20) at 1 and 5 atm. The developed model has also been validated against the literature data which is provided as Supplementary Material. CHEMKIN-PRO [56] was used to carry out the simulations of both ignition delay time and flame speed.

5.1. Shock tube measurements

The ignition delay times measured using five shock tubes and one rapid compression machine are presented here (points in the graphs), together with the model predictions (lines). Ignition delay time definition in the simulations is consistent with that from different facilities. The current mechanism can capture the fuel's reactivity at high temperature (> 1000 K), but at low temperatures the model fails to capture the ignition behavior. As mentioned previously in our discussion of the important reaction classes involved in 1,3-butadiene oxidation, no reliable theoretical or experimental results have been published for the important reactions such as ȮH and HȮ$_2$ radical addition reactions and their subsequent complicated reaction channels. The rate constants in the current version of the model were determined directly from *ab initio* calculations without optimization attempted. Further theoretical or experimen-

tal studies on the important reaction classes of ȮH and HȮ$_2$ radicals adding to 1,3-butadiene and their subsequent first and second O$_2$ addition reactions will be important to improve the model behavior at low- to intermediate- temperatures. Moreover, reliable reaction rate constants calculations on the Ċ$_4$H$_5$-i reacts with O$_2$ and the addition reaction of 1,3-C$_4$H$_6$+Ö will be important in the high temperature chemistry.

Figure 13 shows the effect of pressure on ignition delay times measured in shock tubes and the RCM for fuel in 'air' mixtures at $\varphi = 0.5$, 1.0 and 2.0. The experimental results show that the high-pressure results are correlated with shortened ignition delay times at all equivalence ratios which can be explained with increased reactant concentrations as the pressure goes up. The RCM facility effect from the heat loss after the compression has been taken into consideration in the ignition delay time simulation. The pre-ignition appears to prefer happening on less-reactive fuels which remains a controversy for the cause in the community. It readily contaminates the wall of the shock due to the precursor generation caused by the unsaturated double bond. As a result, the precursor accelerates ignition and results in shorter ignition delay times. To avoid this influence, we have cleaned the shock tube before each shot but the undesired phenomenon still occurs. We thus believe that the physical boundary layer should mainly contribute the
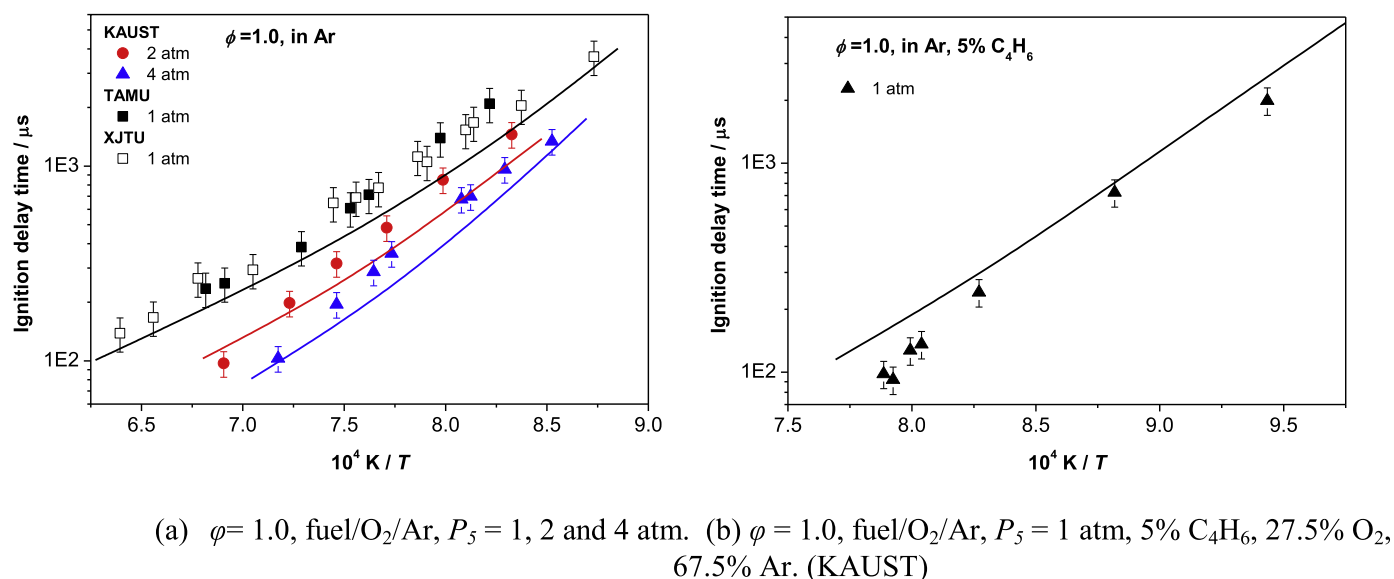
(a) φ= 1.0, fuel/O$_2$/Ar, P_5 = 1, 2 and 4 atm. (b) φ = 1.0, fuel/O$_2$/Ar, P_5 = 1 atm, 5% C$_4$H$_6$, 27.5% O$_2$, 67.5% Ar. (KAUST)

Fig. 16. Ignition delay time measurements and constant volume simulations (solid lines) for $\varphi = 1.0$, fuel/O$_2$/Ar mixtures at different pressures. Experimental measurements from KAUST, TAMU and XJTU.

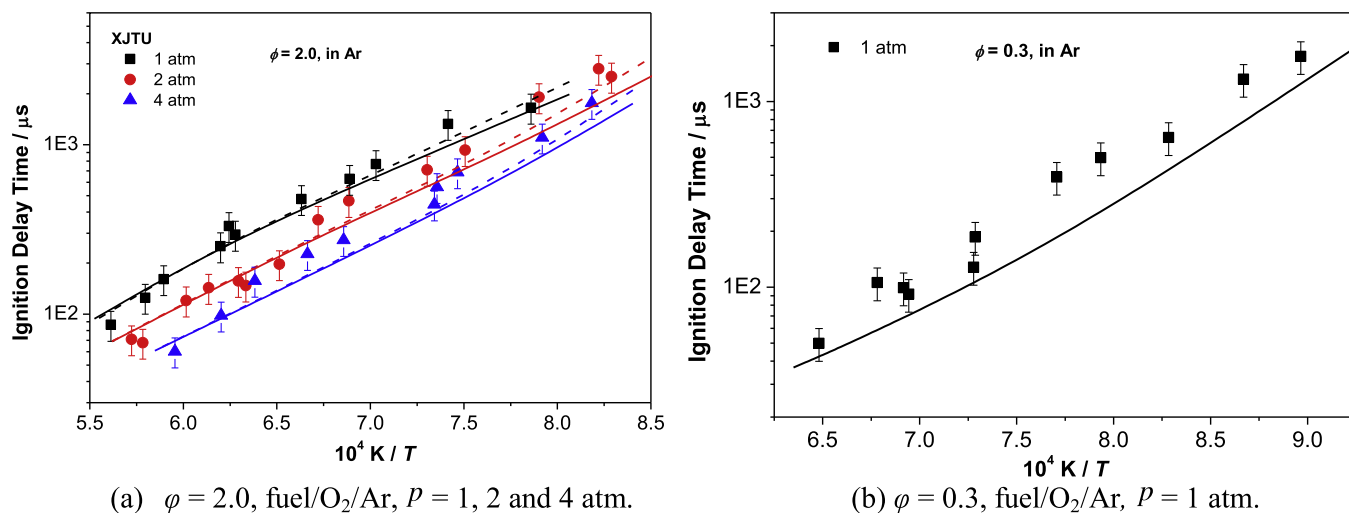(a) φ = 2.0, fuel/O$_2$/Ar, P = 1, 2 and 4 atm.   (b) φ = 0.3, fuel/O$_2$/Ar, P = 1 atm.

Fig. 17. Ignition delay time measurements from XJTU with 4% dp/dt effect simulations (solid lines) and constant volume simulations (dashed lines) for $\varphi = 2.0$ and $\varphi = 0.3$, fuel/O$_2$/Ar mixtures at different pressures.

pre-ignition of 1,3-butadiene while it appears to happen with ignition delay time of 1–2 ms.

Figure 13 shows that the timescale of 1,3-butadiene ignition delay changes dramatically as the equivalence ratio changes from 0.5 to 2.0. Brute force sensitivity for IDTs has been carried out for $\phi = 0.5$ and 2.0 at temperatures of 870 K and 1200 K, shown in Fig. 14. As seen, at 870 K, the addition reactions of ȮH and HȮ$_2$ radicals to 1,3-butadiene and their subsequent reactions play important roles in determining the reactivity of the fuel oxidation. These two reactions are pressure dependent, and sensitivity coefficient changes along with the equivalence ratio. When temperature goes up to 1200 K, the formed important vinyl radical reacts with O$_2$ play an important role in promoting the reactivity. Not surprisingly, the Ö atom adds to 1,3-butadiene is one of the important reactions in determining the fuel reactivity. Branching ratios between the two channels of C$_4$H$_6$ + Ö ⇔CH$_2$O + C$_3$H$_4$-A (inhibiting reactivity) and C$_4$H$_6$ + Ö ⇔C$_2$H$_3$ + CH$_2$CHO (promoting reactivity) along with temperature and pressure changes are important in predicting the fuel reactivity. Further investigations of those important reac-

tion classes are important in determining the final chemistry and the model behavior at different temperature, pressure and equivalence ratio.

Figures 15–18 show the effect of pressure on ignition delay times measured in four different shock tubes for fuel/Ar mixtures at $\varphi = 0.3$, 0.5, 1.0 and 2.0 against the predictions from the current mechanism. The fuel reactivity at high temperatures and low pressures is predicted well by the model. We also found, under the same conditions, that there is a discrepancy between two different facilities. Taking $\varphi = 0.5$ and fuel/Ar mixture as an example, as shown in Fig. 15(a) the black, open squares and the solid squares are at the same equivalence ratio and pressure condition taken by TAMU and UCF separately. The UCF results are consistently faster than those from TAMU but both are within the reported experimental uncertainties. A likely reason for this is the presence of dp/dt and, hence, temperature increases which could make the longer ignition delay times appear accelerated when plotted in a graph such as that in Fig. 15a. For $\varphi = 1.0$ and fuel/O$_2$/Ar mixture, TAMU and XJTU have measured the IDT at the same con-

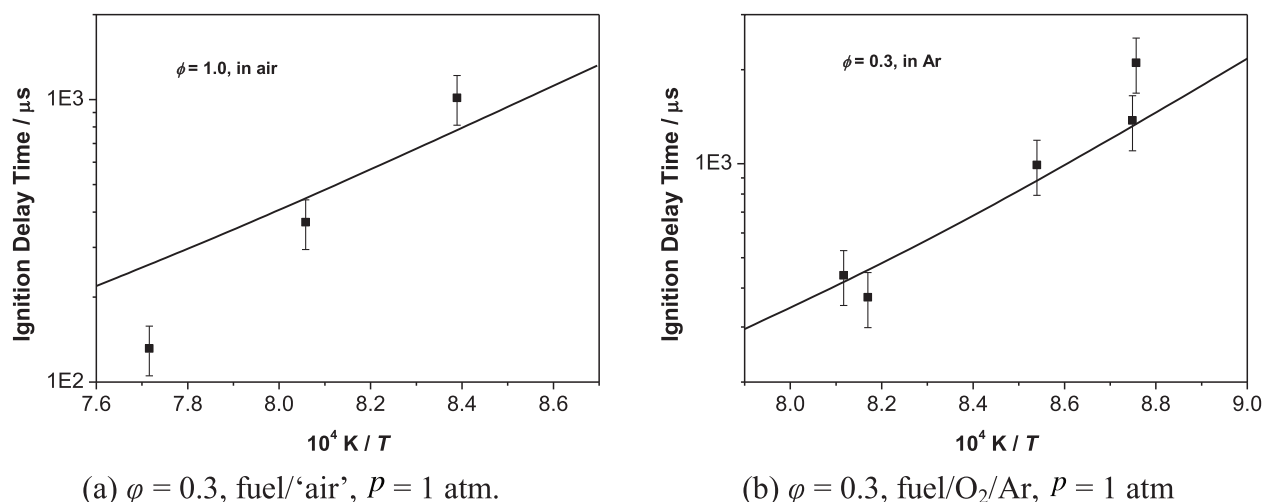(a) $\varphi = 0.3$, fuel/'air', $P = 1$ atm. (b) $\varphi = 0.3$, fuel/O_2/Ar, $P = 1$ atm

Fig. 18. Ignition delay time measurements and constant volume simulations (solid lines) of the UCF data at $\varphi = 0.3$, fuel/'air' and fuel/O_2/Ar mixtures at 1 atm.
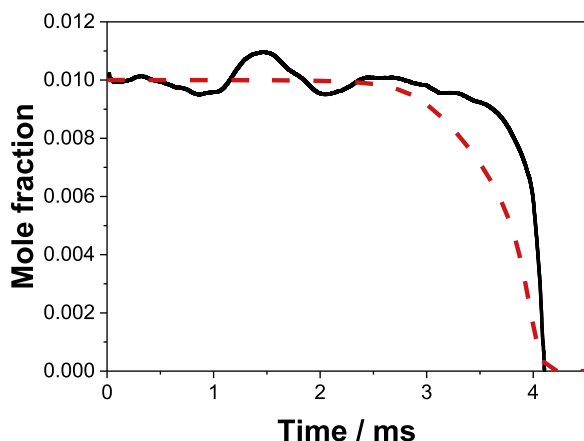

Fig. 19. Mole fraction changes of 1,3-butadiene against time at 1.61 atm and 1091 K for $\varphi = 0.5$ in Ar mixture from UCF measurements. (solid line: experiment, dashed line: simulation).

dition and their experimental results are in very good agreement with each other, Fig. 16(a). The model also gave a relatively good prediction of the experimental results. A comparison of the dp/dt effect on the constant volume ignition delay time simulations of the XJTU data is shown in Fig. 17, where ignition delay times become shorter (solid lines) including this effect compared to those without (dashed lines). The performance of the current mechanism against data shown in Figs. 15–18 can be considered reasonable.

Mole fraction time-histories of 1,3-butadiene measured at UCF are compared against the model simulation at 1.61 atm and 1091 K for $\varphi = 0.5$ and shown in Fig. 19. At the wavelength used (10.537 μm), the main interfering species are alkenes with C=C bonds. A chemical kinetic simulation was performed to estimate the interfering species and it was determined that interference from other alkenes is minimal based on their relative concentrations and absorption cross sections. Regarding line broadening, the absorption cross section at time-zero was characterized for this wavelength for the range of T_5 and p_5 studied. This characterization accounts for the changes in the absorption cross section at the probed wavelength with temperature and pressure, hence broadening is not an issue. As we can see, the model consumes the fuel faster than the experimental measurements after 3 ms which is consistent with the ignition delay time prediction that the model

predicts shorter ignition delay time than the experimental results. The model is in good agreement with the measured data for this particular experiment but not for all of the experimental conditions shown in the Supplementary Material which is consistent with the ignition delay time prediction. Detailed sensitivity analysis and important reaction classes discussion for the discrepancy is shown in Fig. 10.

5.2. Laminar flame speed validation

Figure 20 shows the predicted laminar burning velocities against those measured experimentally for 1,3-butadiene in air at 1 and 5 atm obtained from TAMU. The peak in flame speed is predicted at $\varphi = 1.1$ which is independent of changing temperature and pressure, while the experimentally measured peak changes slightly with temperature at both pressures. At 295 K, the peak in flame speed is located at $\varphi = 1.2$ at both 1 and 5 atm and then changes to $\varphi = 1.1$ at 359 K and 399 K. Overall, there is good agreement between the model prediction and the experimental measurements.

Sensitivity analyses of reaction rate constants to flame speeds for 1,3-butadiene oxidation were performed at 1 and 5 atm at different temperatures and equivalence ratios. Figure 21 shows the results obtained at 5 atm at equivalence ratios of 0.9 and 1.1 at 295 K and 399 K, respectively. Not surprisingly, as for our sensitivity analyses to flame speeds for the butene isomers [1–3], many of the important reactions highlighted there are from the H_2/CO sub-mechanism. Competition between the chain branching reaction of $\dot{H} + O_2 \leftrightarrow \ddot{O} + \dot{O}H$ and the chain propagation reaction of $\dot{H} + O_2 (+M) \leftrightarrow H\dot{O}_2 (+M)$ largely determines the flame speed predictions. The reaction of carbon monoxide with hydroxyl radical is the second most reactivity promoting reaction. These reactions are extremely important in the oxidation of all fuels under different temperatures and pressures. Rate constants for these reactions have been discussed extensively in the previous work by Kéromnès et al. [41]. The highlighted 1,3-butadiene reactions include 1,3-$C_4H_6 + \dot{H} \leftrightarrow C_2H_4 + \dot{C}_2H_3$, C_4H_5-i + $O_2 \leftrightarrow C_2H_3\dot{C}O + CH_2O$. Competition between the chain branching reaction of 1,3-$C_4H_6 + \ddot{O} \leftrightarrow \dot{C}_2H_3 + \dot{C}H_2CHO$ and the chain termination reaction of 1,3-$C_4H_6 + \ddot{O} \leftrightarrow CH_2O + C_3H_4$-a is also important in the flame speed predictions and highlighted here.
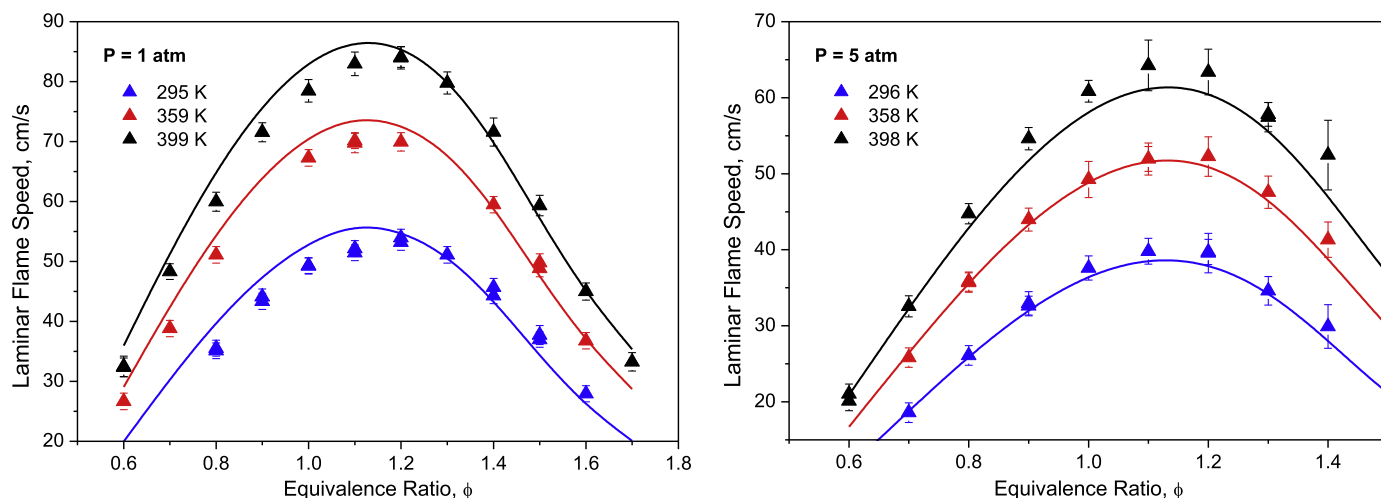
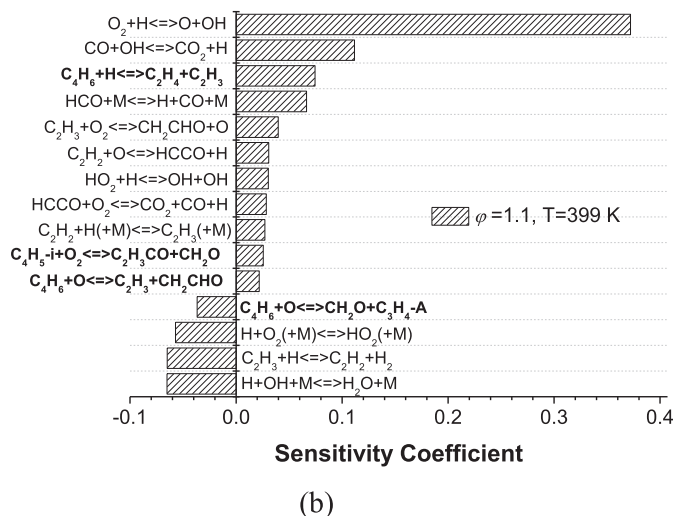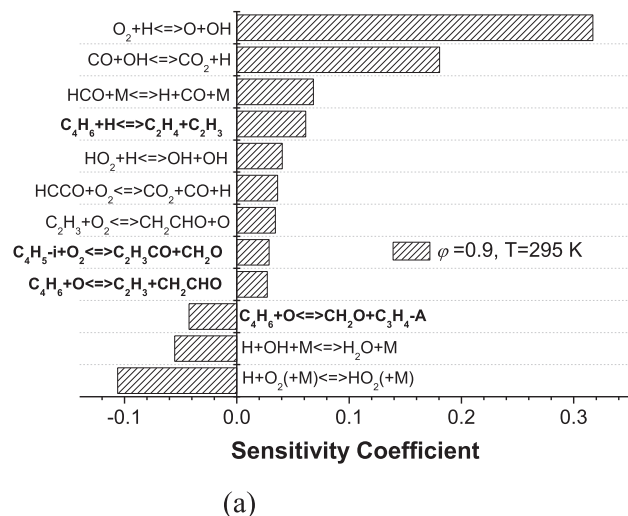**Fig. 20.** Laminar flame speed for 1,3-butadiene in air at 1 and 5 atm. Experimental measurements are from TAMU.

Fig. 21. Flame speed sensitivity analysis at 5 atm for (a) $\varphi = 0.9$, $T = 295$ K, and (b) $\varphi = 1.1$, $T = 399$ K.

6. Conclusions

This paper presents ignition delay time and flame speed measurements of 1,3-butadiene oxidation. The ignition delay times were measured at equivalence ratios of 0.5, 1.0, and 2.0 in 'air' at pressures of 10, 20 and 40 atm in five shock tubes and a rapid compression machine, as well as data at equivalence ratios of 0.3, 0.5, 1.0 and 2.0 in argon, at pressures of 1, 2 and 4 atm in the shock tubes. Laminar flame speeds were measured at 295 K, 359 K and 399 K for 1 and 5 atm over a wide range of equivalence ratios.

A detailed chemical kinetic mechanism has also been developed based on the combination of related literature experimental and theoretical studies, estimates by analogy with alkenes and *ab initio* calculations carried out in this work. The kinetic model includes comprehensive low- and high-temperature reaction mechanisms specific to diene chemistry. The mechanism is validated against our new experimental data with sensitivity analyses used to identify important reaction pathways and kinetic parameters. The current mechanism captures the laminar flame speed measurements quite well and also is in reasonable agreement with high-temperature ignition delay time measurements.

The analogous rate constants from alkenes are used for the important reaction classes involved in 1,3-butadiene low temperature oxidation. These reaction classes are $\dot{O}H$ and $H\dot{O}_2$ radicals

and $^3\ddot{O}$ atom addition to the double bonds in 1,3-butadiene and their subsequent reactions. More studies of these reactions both theoretically and experimentally are important in furthering the understanding of low-temperature oxidation of 1,3-butadiene, and a more concerted effort is required if further strides are to be made in the future.

Supplementary materials

Supplementary material associated with this article can be found, in the online version, at doi:10.1016/j.combustflame.2018.08.006.

References

[1] C.-W. Zhou, Y. Li, E. O'Connor, K.P. Somers, S. Thion, C. Keesee, O. Mathieu, E.L. Petersen, T.A. DeVerter, M.A. Oehlschlaeger, G. Kukkadapu, C.-J. Sung, M. Alrefae, F. Khaled, A. Farooq, P. Dirrenberger, P.-A. Glaude, F. Battin-Leclerc, J. Santner, Y. Ju, T. Held, F.M. Haas, F.L. Dryer, H.J. Curran, A comprehensive experimental and modeling study of isobutene oxidation, Combust. Flame 167 (2016) 353–379.

[2] Y. Li, C.-W. Zhou, K.P. Somers, K. Zhang, H.J. Curran, The oxidation of 2-butene: a high pressure ignition delay, kinetic modeling study and reactivity comparison with isobutene and 1-butene, Proc. Combust. Inst. 36 (2017) 403–411.

[3] Y. Li, C.W. Zhou, H.J. Curran, An extensive experimental and modeling study of 1-butene oxidation, Combust. Flame 181 (2017) 198–213.

[4] R. Fournet, J.C. Bauge, F. Battin-Leclerc, Experimental and modeling of oxidation of acetylene, propyne, allene and 1,3-butadiene, Int. J. Chem. Kinet. 31 (1999) 361–379.

[5] C. Libby, D.F. Davidson, R.K. Hanson, A shock tube study of the oxidation of 1, 3-butadiene, 42nd AIAA Aerospace Sciences Meeting and Exhibit, Reno, NV (2004).

[6] S. Davis, C. Law, Determination of and fuel structure effects on laminar flame speeds of C1 to C8 hydrocarbons, Combust. Sci. Technol. 140 (1998) 427–449.

[7] N. Hansen, J.A. Miller, T. Kasper, K. Kohse-Höinghaus, P.R. Westmoreland, J. Wang, T.A. Cool, Benzene formation in premixed fuel-rich 1, 3-butadiene flames, Proc. Combust. Inst. 32 (2009) 623–630.

[8] M.B. Colket, Pyrolysis of 1, 3-butadiene in a single-pulse shock tube, Eastern States Section Fall Meeting, The Combustion Institute, Providence, RI (1983).

[9] Y. Hidaka, T. Higashihara, N. Ninomiya, H. Masaoka, T. Nakamura, H. Kawano, Shock tube and modeling study of 1,3-butadiene pyrolysis, Int. J. Chem. Kinet. 28 (1996) 137–151.

[10] A. Laskin, H. Wang, C.K. Law, Detailed kinetic modeling of 1,3-butadiene oxidation at high temperatures, Int. J. Chem. Kinet. 32 (2000) 589–614.

[11] K. Brezinsky, E. Burke, I. Glassman, The high temperature oxidation of butadiene, Symp. (Int.) Combust. 20 (1985) 613–622.

[12] P. Dagaut, M. Cathonnet, The oxidation of 1,3-butadiene: experimental results and kinetic modeling, Combust. Sci. Technol. 140 (1998) 225–257.

[13] J.A. Cole, J.D. Bittner, J.P. Longwell, J.B. Howard, Formation mechanisms of aromatic-compounds in aliphatic flames, Combust. Flame 56 (1984) 51–70.

[14] J. Badra, A. Elwardany, F. Khaled, S.S. Vasu, A. Farooq, A shock tube and laser absorption study of ignition delay times and OH reaction rates of ketones: 2-butanone and 3-buten-2-one, Combust. Flame 161 (2014) 725–734.

[15] S.M. Burke, U. Burke, R. Mc Donagh, O. Mathieu, I. Osorio, C. Keesee, A. Morones, E.L. Petersen, W.J. Wang, T.A. DeVerter, M.A. Oehlschlaeger, B. Rhodes, R.K. Hanson, D.F. Davidson, B.W. Weber, C.J. Sung, J. Santner, Y.G. Ju, F.M. Haas, F.L. Dryer, E.N. Volkov, E.J.K. Nilsson, A.A. Konnov, M. Alrefae, F. Khaled, A. Farooq, P. Dirrenberger, P.A. Glaude, F. Battin-Leclerc, H.J. Curran, An experimental and modeling study of propene oxidation. Part 2: ignition delay time and flame speed measurements, Combust. Flame 162 (2015) 296–314.

[16] C.J. Aul, W.K. Metcalfe, S.M. Burke, H.J. Curran, E.L. Petersen, Ignition and kinetic modeling of methane and ethane fuel blends with oxygen: a design of experiments approach, Combust. Flame 160 (2013) 1153–1167.

[17] Y. Zhang, Z. Huang, L. Wei, J. Zhang, C.K. Law, Experimental and modeling study on ignition delays of lean mixtures of methane, hydrogen, oxygen, and argon at elevated pressures, Combust. Flame 159 (2012) 918–931.

[18] Z.E. Loparo, J.G. Lopez, S. Neupane, W.P. Partridge, K. Vodopyanov, S.S. Vasu, Fuel-rich n-heptane oxidation: a shock tube and laser absorption study, Combust. Flame 185 (2017) 220–233.

[19] S.S. Goldsborough, S. Hochgreb, G. Vanhove, M.S. Wooldridge, H.J. Curran, C.J. Sung, Advances in rapid compression machine studies of low- and intermediate-temperature autoignition phenomena, Prog. Energy Combust. Sci. 63 (2017) 1–78.

[20] C.J. Sung, H.J. Curran, Using rapid compression machines for chemical kinetics studies, Prog. Energy Combust. Sci. 44 (2014) 1–18.

[21] J. de Vries, W.B. Lowry, Z. Serinyel, H.J. Curran, E.L. Petersen, Laminar flame speed measurements of dimethyl ether in air at pressures up to 10 atm, Fuel 90 (2011) 331–338.

[22] W. Lowry, J. de Vries, M. Krejci, E. Petersen, Z. Serinyel, W. Metcalfe, H. Curran, G. Bourque, Laminar flame speed measurements and modeling of pure alkanes and alkane blends at elevated pressures, J. Eng. Gas Turbines Power 133 (2011) 091501.

[23] M.L. Frankel, G.I. Sivashinsky, On effects due to thermal expansion and Lewis number in spherical flame propagation, Combust. Sci. Technol. 31 (1983) 131–138.

[24] P.D. Ronney, G.I. Sivashinsky, A theoretical study of propagation and extinction of nonsteady spherical flame fronts, SIAM J. Appl. Math. 49 (1989) 1029–1046.

[25] J.K. Bechtold, C. Cui, M. Matalon, The role of radiative losses in self-extinguishing and self-wrinkling flames, Proc. Combust. Inst. 30 (2005) 177–184.

[26] A.P. Kelley, G. Jomaas, C.K. Law, Critical radius for sustained propagation of spark-ignited spherical flames, Combust. Flame 156 (2009) 1006–1013.

[27] Z. Chen, On the extraction of laminar flame speed and Markstein length from outwardly propagating spherical flames, Combust. Flame 158 (2011) 291–300.

[28] J.A. Montgomery, M.J. Frisch, J.W. Ochterski, G.A. Petersson, A complete basis set model chemistry. VI. Use of density functional geometries and frequencies, J. Chem. Phys. 110 (1999) 2822–2827.

[29] J.A. Montgomery, M.J. Frisch, J.W. Ochterski, G.A. Petersson, A complete basis set model chemistry. VII. Use of the minimum population localization method, J. Chem. Phys. 112 (2000) 6532–6542.

[30] L.A. Curtiss, K. Raghavachari, P.C. Redfern, V. Rassolov, J.A. Pople, Gaussian-3 (G3) theory for molecules containing first and second-row atoms, J. Chem. Phys. 109 (1998) 7764–7776.

[31] L.A. Curtiss, P.C. Redfern, K. Raghavachari, Gaussian-4 theory, J. Chem. Phys. 126 (2007) 12.

[32] S.W. Benson, Thermochemical kinetics, Wiley, 1976.

[33] E.J. Prosen, F.W. Maron, F.D. Rossini, Heats of combustion, formation, and isomerization of ten C4 hydrocarbons, J. Res. NBS 46 (1951) 106–112.

[34] C.F. Goldsmith, G.R. Magoon, W.H. Green, Database of small molecule thermochemistry for combustion, J. Phys. Chem. A 116 (2012) 9033–9057.

[35] S. Furuyama, D.M. Golden, S.W. Benson, Thermochemistry of cyclopentene and cyclopentadiene from studies of gas-phase equilibria, J. Chem. Thermodyn. 2 (1970) 161–169.

[36] J.-D. Chai, M. Head-Gordon, Long-range corrected hybrid density functionals with damped atom-atom dispersion corrections, Phys. Chem. Chem. Phys. 10 (2008) 6615–6620.

[37] D.E. Woon, T.H. Dunning, Gaussian-basis sets for use in correlated molecular calculations. 5. Core-valence basis-sets for boron through neon, J. Chem. Phys. 103 (1995) 4572–4585.

[38] H.J. Werner, Third-order multireference perturbation theory – the CASPT3 method, Mol. Phys. 89 (1996) 645–661.

[39] P. Celani, H.J. Werner, Multireference perturbation theory for large restricted and selected active space reference wave functions, J. Chem. Phys. 112 (2000) 5546–5557.

[40] Y. Li, S.J. Klippenstein, C.W. Zhou, H.J. Curran, Theoretical kinetics analysis for H atom addition to 1,3-butadiene and related reactions on the C4H7 potential energy surface, J. Phys. Chem. A 121 (2017) 7433–7445.

[41] A. Keromnes, W.K. Metcalfe, K.A. Heufer, N. Donohoe, A.K. Das, C.J. Sung, J. Herzler, C. Naumann, P. Griebel, O. Mathieu, M.C. Krejci, E.L. Petersen, W.J. Pitz, H.J. Curran, An experimental and detailed chemical kinetic modeling study of hydrogen and syngas mixture oxidation at elevated pressures, Combust. Flame 160 (2013) 995–1011.

[42] W.K. Metcalfe, S.M. Burke, S.S. Ahmed, H.J. Curran, A hierarchical and comparative kinetic modeling study of C-1–C-2 hydrocarbon and oxygenated fuels, Int. J. Chem. Kinet. 45 (2013) 638–675.

[43] S.M. Burke, W. Metcalfe, O. Herbinet, F. Battin-Leclerc, F.M. Haas, J. Santner, F.L. Dryer, H.J. Curran, An experimental and modeling study of propene oxidation. Part 1: speciation measurements in jet-stirred and flow reactors, Combust. Flame 161 (2014) 2765–2784.

[44] U. Burke, K.P. Somers, P. O'Toole, C.M. Zinner, N. Marquet, G. Bourque, E.L. Petersen, W.K. Metcalfe, Z. Serinyel, H.J. Curran, An ignition delay and kinetic modeling study of methane, dimethyl ether, and their mixtures at high pressures, Combust. Flame 162 (2015) 315–330.

[45] C.F. Goldsmith, W.H. Green, S.J. Klippenstein, Role of O-2 + QOOH in low-temperature ignition of propane. 1. Temperature and pressure dependent rate coefficients, J. Phys. Chem. A 116 (2012) 3325–3346.

[46] R. Sivaramakrishnan, J.V. Michael, Rate constants for OH with selected large alkanes: shock-tube measurements and an improved group scheme, J. Phys. Chem. A 113 (2009) 5047–5060.

[47] J. Zador, A.W. Jasper, J.A. Miller, The reaction between propene and hydroxyl, Phys. Chem. Chem. Phys. 11 (2009) 11040–11053.

[48] C.F. Goldsmith, S.J. Klippenstein, W.H. Green, Theoretical rate coefficients for allyl + HO2 and allyloxy decomposition, Proc. Combust. Inst. 33 (2011) 273–282.

[49] A. Miyoshi, Molecular size dependent falloff rate constants for the recombination reactions of alkyl radicals with O2 and implications for simplified kinetics of alkylperoxyl radicals, Int. J. Chem. Kinet. 44 (2012) 59–74.

[50] S.M. Villano, H.H. Carstensen, A.M. Dean, Rate rules, branching ratios, and pressure dependence of the HO2 + olefin addition channels, J. Phys. Chem. A 117 (2013) 6458–6473.

[51] S. Sharma, S. Raman, W.H. Green, Intramolecular hydrogen migration in alkylperoxy and hydroperoxyalkylperoxy radicals: accurate treatment of hindered rotors, J. Phys. Chem. A 114 (2010) 5689–5701.

[52] S.S. Vasu, J. Zador, D.F. Davidson, R.K. Hanson, D.M. Golden, J.A. Miller, High-temperature measurements and a theoretical study of the reaction of OH with 1,3-butadiene, J. Phys. Chem. A 114 (2010) 8312–8318.

[53] L.K. Rutz, G. da Silva, J.W. Bozzelli, H. Bockhorn, Reaction of the i-C_4H_5 (CH_2CCHCH_2) radical with O_2, J Phys Chem A 115 (2011) 1018–1026.

[54] C. Cavallotti, F. Leonori, N. Balucani, V. Nevrly, A. Bergeat, S. Falcinelli, G. Vanuzzo, P. Casavecchia, Relevance of the channel leading to formaldehyde plus triplet ethylidene in the O(P-3) + propene reaction under combustion conditions, J. Phys. Chem. Lett. 5 (2014) 4213–4218.

[55] J.P.A. Lockhart, C.F. Goldsmith, J.B. Randazzo, B. Ruscic, R.S. Tranter, An experimental and theoretical study of the thermal decomposition of C_4H_6 isomers, J. Phys. Chem. A 121 (2017) 3827–3850.

[56] CHEMKIN-PRO 15101, Reaction design, San Diego, 2013.